TAMPEREEN TEKNILLINEN YLIOPISTO
TAMPERE UNIVERSITY OF TECHNOLOGY

SAMI VALKONEN

COMPARISON OF FAST-CONVOLUTION BASED FILTERED OFDM AND WINDOWED OFDM FOR 5G PHYSICAL LAYER

Master of Science thesis

Examiners: Prof. Mikko Valkama,
D.Sc. Toni Levanen
Examiners and topic approved by the
Faculty Council meeting of
Computing and Electrical Engineering
on 29th March 2017

ABSTRACT

SAMI VALKONEN: Comparison of Fast-Convolution based filtered OFDM and Windowed OFDM for 5G physical layer
Tampere University of Technology
Master of Science thesis, 89 pages
April 2017
Master's Degree Programme in Information Technology
Major: Communication Systems and Networks
Examiners: Prof. Mikko Valkama, D.Sc. Toni Levanen
Keywords: W-OFDM, FC-F-OFDM, 5G, waveforms, NR, CP-OFDM

The demands for modern wireless cellular networks are increasing constantly due to the introduction of new mobile devices and services. Additionally, mobile networks are being used as a primary Internet connection as the current wireless networks are able to achieve similar user experiences than with wired connections in most applications. Long Term Evolution (LTE) and LTE-Advanced are current 4G technologies already allowing very high peak data rates. However, additional features are needed from network to satisfy traffic demands of the future and suitable technologies are in high interest in nowadays research.

The fifth generation (5G) wireless system targets to increase data transmission rates further. In addition, it has been forecast that the traffic trends of the future becomes more delay-critical and small bursts communication has a bigger role. These type of services are e.g. Internet of Things (IoT) and Machine-to-Machine (M2M) communications. These increases dramatically the number of devices connected to Internet, for example smart cars, domestic appliances, sensors and other smart devices, which will require significantly improved capacity and flexibility from the forthcoming mobile communication networks.

In this thesis, two waveform candidates for 5G are evaluated and compared: Windowed CP-OFDM and Fast Convolution based Filtered CP-OFDM. LTE-like channel filtered CP-OFDM is used as a reference in spectral efficiency, power leakage and overall link performance comparisons of the waveforms.

It will be shown that the spectral utilization is improved with proposed waveforms in broadband and narrowband transmissions, which allows higher data rates inside the same bandwidth. The most significant improvement is observed in narrowband power leakage evaluations. Reduced power leakage allows to transmit several narrowband signals with different subcarrier spacings, cyclic prefix lengths, or different timing accuracy with tight frequency spacing without significant interference levels.

TIIVISTELMÄ

SAMI VALKONEN: Nopeaan konvoluutioon perustuva suodatettu OFDM ja ikkunoitu OFDM aaltomuotojen suorituskykyvertailussa 5G fyysiselle kerrokselle
Tampereen teknillinen yliopisto
Diplomityö, 89 sivua
Huhtikuu 2017
Tietotekniikan koulutusohjelma
Pääaine: Communication Systems and Networks
Tarkastajat: Prof. Mikko Valkama, D.Sc. Toni Levanen
Avainsanat: W-OFDM, FC-F-OFDM, 5G, waveforms, NR, CP-OFDM

Nykyisten mobiiliverkkojen vaatimukset kasvavat jatkuvasti, mikä johtuu pitkälti uusien mobiililaitteiden ja -palveluiden suosion kasvusta. Lisäksi matkapuhelinverkkoja on alettu käyttämään pääasiallisena internetyhteytenä, sillä nykyteknologialla on mahdollista saavuttaa kiinteään laajakaistayhteyksiin verrattavia käyttäjäkokemuksia useimmissa sovelluksissa. Nykyiset Long Term Evolution (LTE) ja LTE-Advanced ovat neljännen sukupolven (4G) teknologioita, jotka tarjoavat jo hyvin suuria tiedonsiirtonopeuksia. Tulevaisuuden palvelut vaativat kuitenkin uusia ominaisuuksia verkolta ja tämän takia uusia teknlogioita tutkitaan jatkuvasti lisää.

Viidennen sukupolven (5G) teknologia pyrkii kasvattamaan tiedonsiirtonopeuksia entisestään. Lisäksi on ennustettu, että tulevaisuuden teknologiat vaativat tukea myös pienille ja viivekriittisille lähetyksille, kuten Internet of Things (IoT) ja Machine-to-Machine (M2M) -tyyppisille palveluille. Tämä tarkoittaa, että verkkoon yhdistettyjen laitteiden määrä tulee kasvamaan räjähdysmäisesti. Verkossa ovat jatkossa esimerkiksi älykkäät autot, kodinkoneet, sensorit ja monet muut älykkäät laitteet, mikä vaatii mobiiliverkoilta merkittävästi suurta kapasiteettia ja joustavuutta.

Tässä diplomityössä tutkitaan kahden uuden aaltomuodon soveltuvuutta 5G aaltomuodoksi: ikkunoitu CP-OFDM ja nopeaan konvoluutioon perustuva suodatettu CP-OFDM. Referenssinä on käytetty LTE-tyylistä kanavasuodatettua CP-OFDM aaltomuotoa vertaillen alltomuotojen spektraalista tehokkuutta ja vuototehoa. Aaltomuotojen suorituskykyä vertaillaan lopuksi kokonaisen tietoliikennelinkin yli.

Tulosten perusteella kanavan käyttötehokkuus kasvaa uusilla aaltomuodoilla niin laaja- kuin kapeakaistalähetyksissä, mahdollistaen suurempia tiedonsiirtonopeuksia samassa kanavassa. Parannusta on havaittavissa erityisesti kapeakaistaisten lähetysten vuototehossa. Tämä sallii taajudessa lähekkäin olevien eri alikantoaaltoväliä, eri mittaisia syklisiä etuliitteitä tai eri aikasynkronisuusvaatimuksia käyytävien signaalien lähettämisen samanaikaisesti, häiritsemättä merkittävästi muita lähetyksiä.

PREFACE

This thesis is done as a part of a 5G research project of Nokia and the Faculty of the Electronics and Communications Engineering of Tampere University of Technology. I have researched 5G physical layer and especially parameters of different waveform candidates. This thesis are based on results of my daily work as a subcontractor at Nokia's Tampere office.

Thesis project started in June 2016 while i was simultaneously working full-time. The progress was rather slow and in January 2017 I decided to allocate more time for writing this paper. That was a turning point for progression of this thesis and eventually the thesis was complete in the beginning of the April 2017.

I would like to thank D.Sc Toni Levanen for constructive and fast feedback and Prof. Mikko Valkama for final comments. In addition, my family and friends have supported me while having hard times with writing this thesis, which I appreciate very much.

Tampere, 17.4.2017

Sami Valkonen

TABLE OF CONTENTS

LIST OF FIGURES

LIST OF TABLES

LIST OF ABBREVIATIONS AND SYMBOLS

1-dBp	1 dB compression point
1G	1st Generation
2G	2nd Generation
3G	3rd Generation
3GPP	3rd Generation Partnership Project
4G	4th Generation
5G	5th Generation
ACLR	Adjacent Channel Leakage Ratio
AFB	Analysis Filter Bank
AM-AM	Amplitude-to-amplitude
AM-PM	Amplitude-to-phase
BLER	Block Error Rate
BO	Back-off
BS	Base Station
BW	Bandwidth
CP	Cyclic Prefix
DFT	Discrete Fourier Transform
DFTs-OFDM	DFT spread OFDM
DL	Downlink
ECP	Extended Cyclic Prefix
eMBB	enhanced Mobile Broadband
EVM	Error Vector Magnitude
FBMC	Filter Bank Multicarrier
FC	Fast Convolution
FC-F-OFDM	Fast Convolution Filtered OFDM
FDMA	Frequency Division Multiple Access
FFT	Fast Fourier Transform
FIR	Finite Impulse Response
F-OFDM	Filtered OFDM
GB	Guard Band
GP	Guard Period
GSM	Global System for Mobile Communication
IBO	Input Back-off
ICI	Intercarrier Interference
IDFT	Inverse Discrete Fourier Transform

IFFT	Inverse Fast Fourier Transform
IoT	Internet of Things
ISI	Inter Symbol Interference
LTE	Long Term Evolution
M2M	Machine-to-Machine
MCS	Modulation and Coding Scheme
MIMO	Multiple-input, multiple-output
MTC	Machine-type-communication
NR	New Radio
OBE	Out-of-band Emission
OFDM	Orthogonal Frequency Division Multiplexing
OLA	Overlap and Add
OLS	Overlap and Save
OOB	Out-of-band
OQAM	Offset Quadradure Amplitude Modulation
PA	Power Amplifier
PAPR	Peak-to-Average Power Ratio
PRB	Physical Resource Block
PSD	Power Spectral Density
PSK	Phase Shift Keying
QAM	Quadrature Amplitude Modulation
QPSK	Quadrature Phase Shift Keying
RAN	Radio Access Network
RC	Raised Cosine
RMS	Root Mean Square
Rx	Receiver Side
SC	Subcarrier
SCS	Subcarrier Spacing
SFB	Synthesis Filter Bank
SISO	Single-input single-output
SNR	Signal-to-noise ratio
TBW	Transition Bandwidth
TDD	Time Division Duplexing
TDL	Tapped Delay Line
Tx	Transmitter side
UE	User Equipment
UF-OFDM	Universal Filtered OFDM

UFMC	Universal Filtered Multicarrier
UL	Uplink
UMTS	Universal Mobile Telecommunications System
URLLC	Ultra Reliable Low Latency Communication
V2X	Vehicle-to-Everything
W-OFDM	Windowed OFDM
WOLA	Weighted Overlap and Add

LIST OF SYMBOLS

α	Roll-off factor
$\delta(.)$	Dirac delta function
Δf	Subcarrier Spacing
$\theta_m(r)$	Phase rotation of mth subband
λ	Overlapping factor
μ_N	Number of multiplications required for N-size FFT/IFFT
τ_i	TDL multipath delay if ith component
Ω	Load of the PA
$A_c(\tau)$	Power delay profile
$\bar{\tau}$	Mean of access delay
B	Bandwidth
C_x	Total number of real multiplications required for x
c_i	TDL multipath coefficient fot ith component
$\mathbf{D}_m$	Weight matrix for mth subband
$\mathbf{F}_{m,r}$	Synthesis sub-block matrix
$\mathbf{F}_m$	Block diagonal matrix
$\mathbf{G}_{m,r}$	Analysis sub-block matrix
F_S	Sampling Rate
H_m	Sampling Rate reduction factor for subband m
I_m	Sampling Rate conversion factor for subband m
L_m	Block length in SFB processing for mth subband
$L_{S,m}$	Number of non-overlapping input samples in SFB
$\bar{L}_m$	Block length in Analysis Filter Bank Processing
$\bar{L}_{S,m}$	Number of non-overlapping input samples in AFB
M	Number of subbands
$\mathbf{M}_{m,r}$	Frequency domain mapping matrix
N	Long transform size in FC-processing
N_{ACT}	Number of active subcarriers
N_{CP}	Length of CP in samples
N_{ECP}	Length of extended CP in samples
N_{ext}	Length of extended part of the symbol in samples
N_{FFT}	FFT size in samples
N_{NO}	Number of non-overlapping samples
N_S	Number of subcarriers
N_{SYM}	Number of symbols

N_{NO}	Number of non-overlapping output samples
N_{ws}	W-OFDM window size in symbols
N_{W-OFDM}	Length of W-OFDM symbol in samples
p_x	xth polynomial coefficient
$P_{adjacent}$	Average power of adjacent channel
$P_{assigned}$	Average power of assigned allocation
$\mathbf{P}_{L_m}^{(L_m/2)}$	Circular permutation matrix of SFB
$\mathbf{P}_{N}^{(N/2)}$	Circular permutation matrix of AFB
P	Smoothness factor for RAPP PA model
P_{ave}	Measured output power level of PA
P_{max}	Maximum output power of the PA
P_{target}	Target PA input power
Q	Smoothness factor for RAPP PA model
R	Coding Rate
$\mathbf{S}_{\bar{L}_m}$	Selection matrix for AFB
$\mathbf{S_N}$	Selection matrix for SFB
T_{CP}	CP duration in time units
T_{ext}	Symbol extension duration in time units
$T_{\text{FC-BLOCKS},m}$	Number of FC Tx processing blocks
T_{FFT}	FFT size in time units
T_{OL}	Overlap presented in time units
T_u	Symbol duration in time units
T_W	W-OFDM window duration in time units
T_{W-OFDM}	W-OFDM symbol duration in time units
V_{SAT}	Saturation voltage of PA
$\mathbf{W}_{L_m}$	FFT matrix for AFB
$\mathbf{w}_m$	Transmitter sub-block matrix
$\mathbf{W}_N$	FFT matrix for SFB
$\mathbf{W}_N^{-1}$	IFFT matrix for SFB
$\mathbf{W}_{\bar{L}_m}^{-1}$	IFFT matrix for AFB
x	Input signal
y	Output signal

1. INTRODUCTION

The evolution of the digital mobile communication technologies has followed a trend that a new generation is introduced approximately once a decade [1]. After the first analog generation (1G), the second generation (2G), GSM, became widespread around 1990 and offered digital voice services world-wide. The third generation (3G), UMTS, released around 2000, included already a data service in its initial design. Later on, it was extended with HSPA technology, which made the network architecture all-IP based. As the fourth generation (4G), called as Long Term Evolution (LTE), offered world-wide broadband data-services, the vision of the ubiquitous Internet started to become realistic [2].

Wireless data traffic is forecasted to grow dramatically, during the next 20 years. That is due to the high data rate applications, such as ultra-high resolution video streaming, cloud-based work, and high quality entertainment applications [3]. New mobile devices such as smart phones and tablets have brought new applications to customers, which are allowed by the rapid evolution of wireless cellular networks. Increasing performance of wireless internet connections has also enabled to use it as a primary connection to the Internet in several areas, which has increased the wireless cellular network data traffic requirements further. However, traditional cellular access bands below 6 GHz are already mainly in use for licenced users forcing the fifth generation (5G) development to exploit higher frequencies between 6 GHz and 100 GHz [3]. This range can be split in two parts: centimeter wave and millimeter wave, based on different radio propagation characteristics. Hence, more New Radio (NR) access technologies will be needed to address this regime of frequency bands due to different channel characteristics.

To meet the future traffic demands, 5G cellular network research targets to remarkably higher peak data rates and lower latency experience than current 4G network provides. While it is almost impossible to forecast the killer application of 2025, it is anticipated that the Tactile Internet, Internet of Things (IoT) and machine-type-communication (MTC) will play an important role in shaping the traffic profile experienced in the future wireless communication networks [1, 4]. These new traffic types have new characteristics, such as sporadic in nature, timing mis-

alignment, small packets and huge numbers of communication devices. Hence, in order to serve these mixed low data rate services inside a single wideband channel, support for the mixed synchronous and asynchronous traffic scheme is needed [4, 5, 6, 7]. Other expected feature for 5G is to support for ultra-reliable ultra-low latency (URLLC) services, such as Vehicle-to-Everything (V2X) communications, where the passengers safety relies on the network [5, 6]. LTE system was not designed to meet aforementioned characteristics and 5G design is driven strongly to serve the aforementioned new trends in wireless data traffic.

Orthogonal frequency-division multiplexing (OFDM), which is already used in 4G cellular network, is a suitable solution for high bit rate mobile broadband communications especially with cyclic prefix (CP-OFDM). Nevertheless, CP-OFDM signal has relatively high side lobes in spectrum, which causes power leakage to adjacent channels and more guard bands are needed degrading the spectral efficiency. A usage of a power amplifier (PA) increases the power leakage further, and thus, it is necessary to study effects of transmitter PA non-linearities on the spectrum localization of the waveforms. That is why the channel filtering is applied on top of the CP-OFDM technique in LTE solution in order to satisfy out-of-band emission requirements. When using unused frequency spectrum cap below 6 GHz, which are typically strictly band limited, the spectral efficiency becomes a crucial factor to achieve reasonable data rates. Therefore, the basic CP-OFDM or channel filtered CP-OFDM are not very suitable for exploiting small gaps between licenced bands, which is predicted to play bigger role in the future wireless communication [8].

Suppressing side lobes of CP-OFDM signal has gained high interest in recent research, because it allows to use narrow guardbands between different channels as well as frequency division multiple access (FDMA) with non-synchronized transmission in adjacent frequency slots [8]. As a result the spectrum efficiency of the used channel in increased, which enables higher data rate transmissions. Most probably the 5G waveform will include CP-OFDM with some power leakage reduction enhancements in some form. Currently the most attractive solutions seems to be CP-OFDM with some form of filtering or time domain windowing. [9]

In this thesis, Fast Convolution Filtered CP-OFDM (FC-F-OFDM) is considered as a proper solution for efficient filtered CP-OFDM scheme based of Fast Convolution processing. Filtering adds complexity to the transmitter (Tx) and receiver (Rx) processing and the trade-off between better spectral localization and higher complexity is also discussed. Shaping OFDM symbol in time domain is a low-complex method for reducing intercarrier interference (ICI) caused by power leakage.

Windowed CP-OFDM (W-OFDM) waveform, which utilizes well-known Windowed Overlap and Add (WOLA) -processing, is also one potential candidate for 5G waveform [10], based on time domain windowing [11]. Several windows can be used for symbols in different subcarriers as introduced in [12]. However, single window scheme is applied in this thesis, that is, the same window is used for all subcarriers keeping the implementation complexity as low as possible.

The scope of this thesis is to compare improvements of FC-F-OFDM and W-OFDM against the current LTE waveform in terms of transmitter side and overall link performance. The evolution of spectral efficiency, which can be utilized as a wider transmission bandwidth, is examined with illustrations of Power Spectral Density (PSD) plots showing the performance of the sidelobe suppression techniques. W-OFDM and FC-F-OFDM are techniques are also investigated in a practical case study using the 10 MHz 3GPP LTE channel in order to evaluate BLER link performances in four different 5G relevant transmission scenarios including interference-free, mixed numerology interference and asynchronous interference schemes. Power amplifiers are included in the evaluations as it has a significant effect to the transmitted signal spectrum, and thus, to the overall outcomes. In addition, the possible side effects are discussed in terms of computational complexity and output power consumption.

This thesis is structured as follows: In Chapter 2, the principles of the OFDM are explained in details and the CP extension in introduced. The signal processing of W-OFDM and FC-F-OFDM waveforms are described thoroughly in Chapters 3 and 4, respectively. Filtering and Windowing techniques are illustrated with examples and the reasons to use these waveforms are given. In Chapter 5, the link simulation tool is reviewed in terms of channel parameters and conditions. Selected waveform specific parametrization with arguments are represented as well. Transmitter side performance in terms of spectral localization and adjacent channel leakage ratio (ACLR) are presented in Chapter 6. In Chapter 7, the link performance results are shown in four different 5G relevant transmission cases with aforementioned 5G NR related interference schemes. The results are then discussed through and the suitability of the proposed techniques for 5G solution are estimated and improvements compared to current LTE solution are highlighted. In Chapter 8, all results are concluded and the topics of the thesis are gathered together.

2. ORTHOGONAL FREQUENCY DIVISION MULTIPLEXING

In this chapter, *Orthogonal Frequency Division Multiplexing* (OFDM) is introduced with *Cyclic Prefix* (CP) extension, which is the baseline for waveforms concerning this thesis. The main focus is to describe OFDM fundamentals thoroughly, which are orthogonality, IFFT/FFT implementation and the use of CP. The general mathematical formulation of OFDM scheme is concluded, which is extended with additional waveform processing techniques in Chapters 3 and 4. It is essential to acquire a basic understanding of the OFDM system because it is utilized in the current LTE downlink solution and is the baseline for 5G New Radio (NR) waveform [13]. CP-OFDM waveform with LTE-like channel filtering (explained in more details in Chapter 5) is considered as a reference waveform in this thesis. It should be noted that all practical systems use windowing or filtering in some form with CP-OFDM to fulfill LTE out-of-band (OOB) emission requirements. In Chapter 6 and 7, all results of the new proposed waveforms are compared to LTE-like channel filtered CP-OFDM waveform. The purpose of this chapter is to give basic understanding of CP-OFDM waveform and ensure the understanding of improvements in enhanced CP-OFDM waveforms discussed in Chapters 3 and 4, which are implemented on top of CP-OFDM technique.

2.1 Introduction to OFDM technique

In an OFDM system, the available bandwidth (BW) is divided into multiple overlapping subcarriers (SC) and it can be considered as a special case of a multicarrier transmission. High-rate data stream is converted into several low-rate data streams, which are modulated with separate symbol and transmitted parallel over multiple narrowband channels. The combination of subcarriers enables to achieve similar data rates than in conventional single carrier modulation schemes within equivalent bandwidths.

The basic principle is that subcarriers are mathematically orthogonal to each other meaning that at active carrier frequencies, value of other subcarriers goes

to zero. Therefore, they do not cause interference to other subcarriers, called as *Intercarrier Interference* (ICI)[1], even though they overlap in frequency domain as seen in Figure 2.2 (b). This allows to locate subcarriers closer to each other in the frequency increasing the spectral efficiency compared to conventional multicarrier transmission scheme (shown in Figure 2.1). Subcarrier spacing (SCS), denoted as $\Delta f = 1/T_u$, indicates a frequency gap between adjacent subcarriers, where T_u is the symbol duration in time (demonstrated in Figure 2.2 (a)). The whole bandwidth B can be expressed as

$$B = N_s * \Delta f \tag{2.1}$$

where N_s is a number of subcarriers.

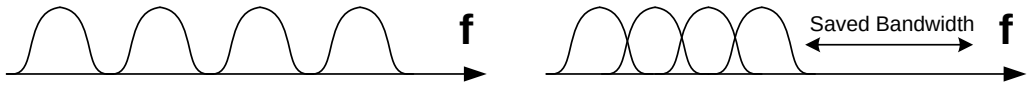

(a) Conventional multicarrier transmission. (b) Orthogonal multicarrier transmission.

Figure 2.1 *Saved bandwidth gained with orthogonal multicarrier technique.*

OFDM systems use rectangular pulse shaping in time domain which corresponds to a *sinc* function in frequency domain. Figure 2.2 (a) demostrates OFDM symbol and Figure 2.2 (b) four consecutive OFDM subcarriers, that is, sinc pulses in frequency domain. *Sinc* function is defined as $\text{sinc}(x) = \sin(x)/x$. Therefore, OFDM signal is a sum of *sinc* pulses resulting accumulation of *sinc* side lobes. This causes high powered side lobes outside the active subcarriers, as shown in Figure 2.2 (b). It should be noted that the first side lobe of the sinc pulse is attenuated only 13 dB with respect to peak power (see Figure 2.2) (b). If the subcarrier power is constant in OFDM signal, the first side lobe is also 13 dB lower with respect to average inband power.

2.1.1 OFDM Signal Structure

As mentioned in 2.1, an OFDM signal consists of multiple sinc-shaped subcarriers in frequency domain that are usually modulated using *Phase Shift Keying* (PSK) or *Quadrature Amplitude Modulation* (QAM) [14]. Lets assume that s_i are N_s random independent complex QAM symbols $\{s_0, s_1, s_2, ..., s_{N-1}\}$ and T_u is the useful symbol

[1]ICI takes place in OFDM system e.g. in presence of frequency offset, when orthogonality is lost and adjacent subcarriers are not zero-valued at sampling time instant of current subcarrier (see Figure 2.2). Frequency offset is discussed further in Section 2.2.2.

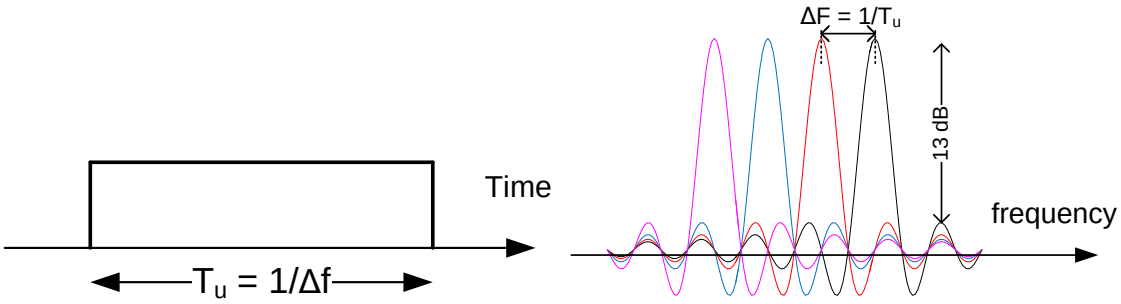

(a) OFDM pulse shape in time domain.

(b) Spectrum of four consecutive OFDM subcarriers.

Figure 2.2 *OFDM pulse shape in (a) time and (b) frequency domain.*

duration. OFDM modulator consist of a bank of N_s complex modulator [15] as illustrated in Figure 2.3. OFDM modulates each symbol to complex subcarriers $\phi(t) = e^{j2\pi f_k t}$. A single modulated subcarrier becomes:

$$x_k(t) = s_k e^{(j2\pi f_k t)}, \tag{2.2}$$

where $f_k = \Delta f * k$ is frequency of kth subcarrier.

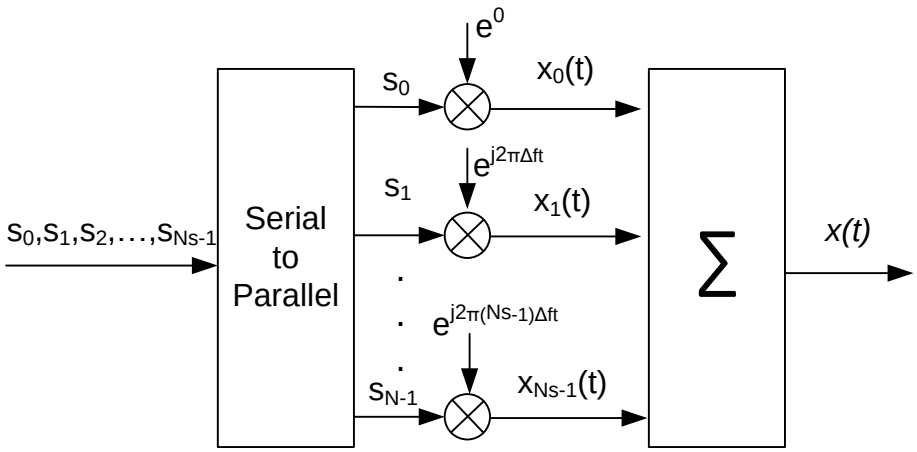

Figure 2.3 *Basic principle of OFDM signal generation through a bank of modulators.*

As discussed in 2.1, the OFDM signal is a sum of N_s subcarriers. Therefore, the OFDM signal can be expressed as a sum of subcarriers modulated by QAM symbols as follows:

$$x(t) = \sum_{k=0}^{N_s-1} s_k e^{(j2\pi\Delta f_k t)} \tag{2.3}$$

The complex OFDM modulated symbols $x(t)$ are actually just frequency shifted data symbols x_i. Subcarrier frequencies, determined as

$$f_k = k\Delta f, \tag{2.4}$$

indicates those frequency shifts, which have to be multiples of $1/T_u$ to achieve orthogonality between subcarriers. The best efficiency is achieved with the smallest possible subcarrier spacing $\Delta f = 1/T_u$.

2.1.2 Fast Fourier Transform based OFDM

In practice, the OFDM signal can be modulated and demodulated using N_{FFT} size *Inverse Fast Fourier Transform* (IFFT) *Fast Fourier Transform* (FFT)[2]. OFDM allows for low complexity implementation by means of computionally efficient FFT processing. Data symbol are converted to the parallel form and mapped to input bins of an IFFT processing block which converts the frequency domain symbols to time domain symbol as illustrated in Figure 2.4.

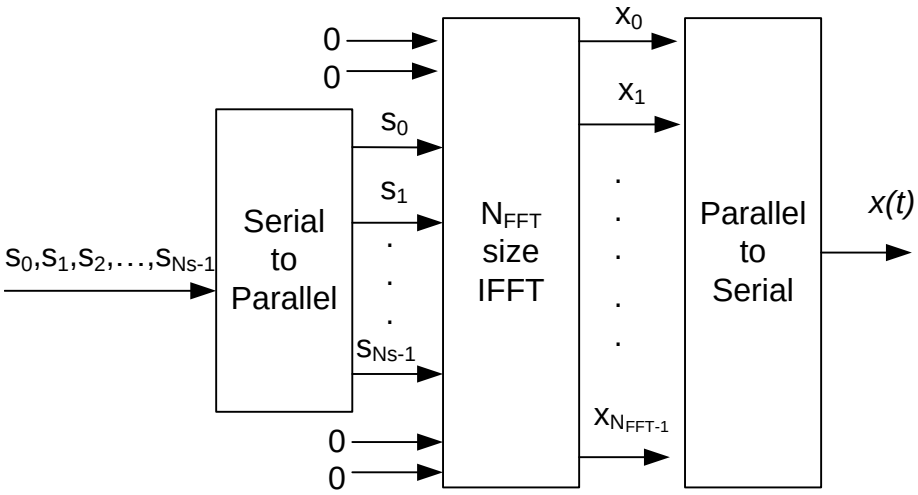

Figure 2.4 *OFDM signal generation by IFFT processing.*

It can be seen that N_s data symbols are IFFT inputs and in generic case initial symbol block is extended with $N_{\mathrm{FFT}} - N_s$ zeros to ensure N_{FFT} size input for IFFT processing block. Sufficient amount of zeros in the transform allows to simplify channel filtering used in LTE (explained in Section 5.1.1). Then parallel to

[2]FFT algorithm computes the discrete Fourier transform (DFT) of a sequence and is used here to indicate DFT operation

serial -converter forms one OFDM symbol of N_s samples. To implement OFDM efficiently, N_{FFT} should be selected equal to 2^m for some integer m. This allows to use implementation-efficient radix-2 IFFT/FFT processing [14].

2.1.3 Concept of Cyclic Prefix

Efficient way to deal with multipath delay spread is one of the most attractive advantages of OFDM. Delay spread can be interpreted as the difference between the time of arrival of the earliest significant multipath component and the latest multipath component. When receiver sees multiple delayed replicas of the transmitted signal, the orthogonality between subcarriers will be lost, shown in Figure 2.5. Dividing the input data stream into N_s subcarriers makes the symbol duration N_s times longer in time domain, which also reduces the relative multipath delay spread [14]. A guard time is introduced in OFDM to eliminate *Intersymbol Interference* (ISI).

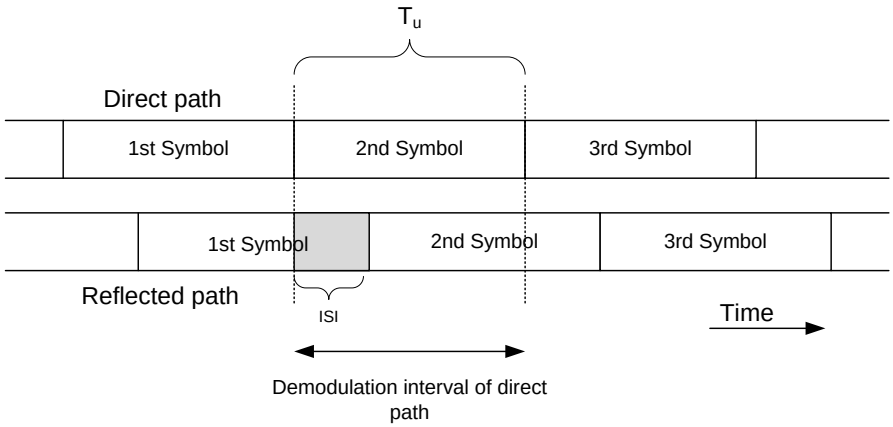

Figure 2.5 *Received signal timing in presence of one multipath component.*

To maintain orthogonality between subcarriers, Cyclic Prefix is used as a guard time for OFDM symbol. CP is a copy of $N_{\mathrm{CP}} = T_{\mathrm{CP}}/F_S$ latest samples of symbol, inserted to the beginning of the initial symbol. Unlike adding zeros, this does not cause any discontinuities to symbol as shown in Figure 2.6. For each OFDM symbol, CP is chosen longer than the time dispersion caused by the channel (delay spread). However, that increases symbol time from T_u to $T_u + T_{\mathrm{CP}}$, where T_{CP} is the length of the cyclic prefix in time. Consequently total overhead of the symbol increases reducing maximum achievable bit rate of the transmission. Nevertheless, due to CP insertion it is possible to receive symbols correctly although existence of multipath components (not longer than CP). At the receiver side, corresponding N_{CP} samples are discarded before FFT processing.

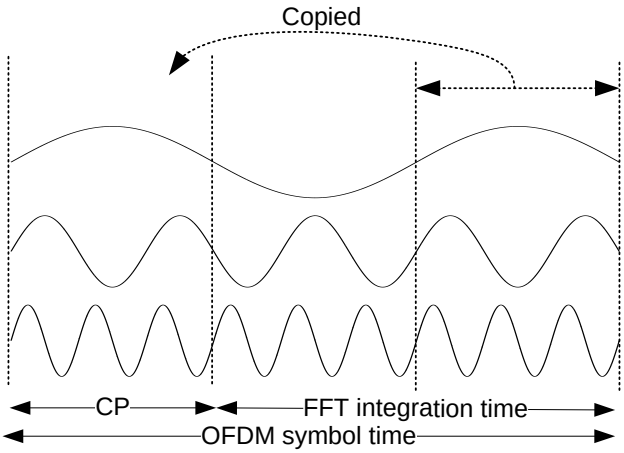

Figure 2.6 *Illustration of cyclic prefix added to OFDM symbol with different frequencies.*

2.2 Advantages and Drawbacks of OFDM

Orthogonal frequency division multiplexing has many potential and useful properties for wireless high data rate communications compared to conventional single carrier transmission scheme. However, OFDM is not perfect solution for all type of communications: It has also some drawbacks, which can be critical for certain type of requirements.

2.2.1 Advantages

As discussed in 2.1, OFDM allows overlapping of orthogonal subcarriers which can be utilized for efficient spectrum use without interfering other subcarriers (shown in Figure 2.1). Hence, no quard band are required between subcarriers which further improves spectral efficiency. This can be implemented with low complexity using IFFT processing as discussed in Section 2.1.2, which efficiently maintains the orthogonality between subcarriers.

High robustness against frequency selective fading is one of the main reasons to use OFDM [14]. In a highly frequency-selective channel in case of single carrier transmission, each symbol is transmitted over frequency bands with multiple different instantaneous channel qualities (referred as *frequency diversity*) as illustrated in Figure 2.7 (a). In OFDM transmission, each symbol is mainly confined to relatively narrow bandwidth. Hence, certain symbols may experience very low instantaneous channel quality (see Figure 2.7 (b)). Therefore, individual symbols typically do not experience significant frequency diversity. However, some subcarriers may have critically poor channel conditions for successful communications. *Frequency inter-*

leaving is used for distributing bits in frequency domain to minimize the effect of failed subcarriers.

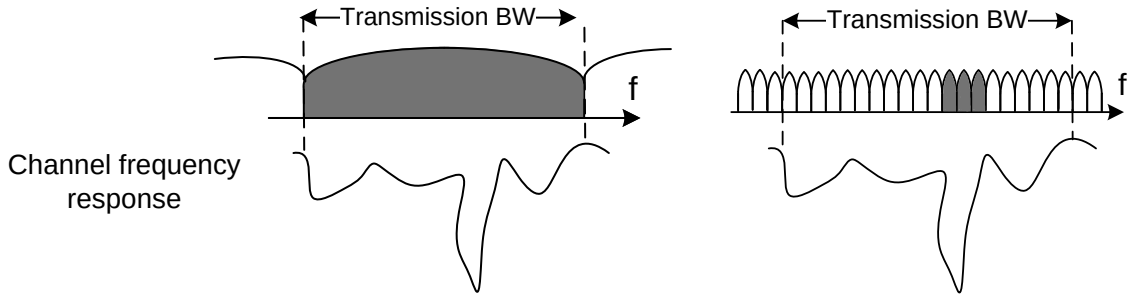

(a) Single carrier wideband transmission (b) OFDM multicarrier transmission

Figure 2.7 *(a) Single carrier and (b) multicarrier transmission in frequency selective channel. Violated carriers are highlighted with grey.*

Dividing wide band channel into multiple subchannels simplifies also channel estimation and equalization assuming that CP is longer than channel delay spread (recall Section 2.1.3). Typically each narrowband subcarriers have practically constant channel frequency response. Instead of estimating whole bandwidth, one tap frequency domain estimator and equalizer can be used for each subcarrier frequency to compensate the effect of channel. Besides, the spectral fragmentation provides adaptive transmission techniques for separate subcarriers. It is easy to multiplex several users in frequency domain by allocating different subcarriers for each user. As the wide band channel is divided into pieces, it is possible to avoid using subchannels suffering significantly poorer channel conditions in order to obtain multiplexing gain. In case of single wideband transmission, the whole carrier is violated (see Figure 2.7 (b)) requiring complex channel equalization structure. In Figure 2.7 (b), subcarriers and corresponding channel frequency response is illustrated. Subcarriers having very low channels frequency response are colored in grey and are unused for this particular user.

In addition, usage of multiple-input multiple output (MIMO) antenna scheme is flexible with OFDM to improve further system performance. Subchannel separation in OFDM is extra beneficial in MIMO detection, where channel is more complicated [16]. For example, a set of subcarriers can be allocated for each transmit antenna allowing multiple simultaneous transmission, which increases the data rate. However, multiantenna techniques are not considered in the scope of this thesis, but is a interesting topic for future research based on the results presented here.

2.2.2 Drawbacks

OFDM have many attractive features as discussed in Section 2.2.1. However, it has also some drawbacks and undesired features to be consider when designing OFDM system, which are discussed in this section.

Firstly, pure OFDM signal has relatively high side lobes (see Figure 2.8) in spectrum, which is unsatisfactory feature for the future communications systems [17]. These high side lobes are generated because of sinc-shaped pulse as stated in Section 2.1. It is well known that the peak of the first side lobes is only 13 dB below the peak of its main lobe [18] as shown in Figure 2.8. As the mixed numerology and asynchronous traffic types (explained in Chapter 7) inside a one channel bandwidth are in high interest of the 5G communication system research, the side lobes should be small not to interfere with other adjacent signals inside a channel. In order to avoid interference caused by side lobes, guard bands are introduced around OFDM signal which reduces the spectral efficiency of the transmission. Also many OFDM side lobe suppression methods have been proposed [9, 12, 19] to resolve this problem and is the main scope area in this thesis as well.

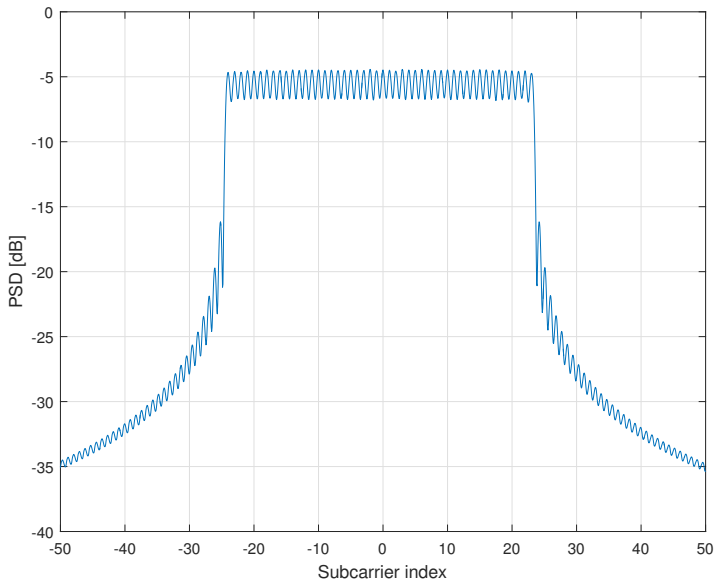

Figure 2.8 *Spectrum of the OFDM signal with 48 active subcarriers.*

Other considerable drawback is high *Peak-to-Power Average Ratio* (PAPR) of OFDM signal which is resulting also in the nature of OFDM symbol sinusoidal waves. At some time instances, sinusoids add up coherently in phase and produces

high peak value compared to average power level, which causes high PAPR values. PAPR is defined as

$$\mathrm{PAPR}[x(t)] = \frac{\max[x(t)^2]}{x_{\mathrm{rms}}}, \tag{2.5}$$

where $x(t)$ is the considered signal and x_{rms} is the root mean square of the $x(t)$.

Transmitter power efficiency is a crucial metric for future wireless communication systems [8]. In order to achieve a sufficient power efficiency, the power amplifier (PA) requires to operate close to its saturation level, which is problematic especially when multicarrier waveforms with high PAPR are used. This leads to high spectral spreading in PA output, which significantly reduces the spectral efficiency [20] [21]. Therefore, in presence of high PAPR values, non-linear distortion is likely to take place in the transmitter PA [22], which makes PA design challenging (explained in more details in Chapter 5.4). Problems takes place especially in uplink (UL)[3] direction, where transmitter equipment is size-restricted mobile terminal. In downlink (DL)[4], in which the transmitter equipment is located in the base station, power amplifier performance can be improved by increasing the size of a PA. Furthermore, complexity of digital-to-analog and analog-to-digital converters increases as well with high PAPR values [23].

Lots of PAPR reduction mechanisms have been researched to improve PA output performance of multicarrier waveforms, but those mechanisms are out of scope of this thesis. Some PAPR reduction techniques are presented in [8], [24] and [25].

OFDM signal is also sensitive to phase noise and frequency offsets, usually caused by impairments of the local oscillator [26]. Phase noise causes leakage of FFT, which subsequently destroys the orthogonality among subcarrier signals, which results in as common phase error and ICI for OFDM signal [27]. Frequency offset shifts the frequency sampling point leading to ICI as shown in Figure 2.9. Hence, synchronization of the carrier frequency at the receiver must be performed very accurately to prevent losing orthogonality between the subcarriers. Even a small frequency offset is significant, if the subcarrier spacing is small, that is, subcarriers are packed close to each other. If the orthogonality is lost, FFT output for each subcarrier will contain interfering terms from all other subcarriers as illustrated in Figure 2.9. The frequency offset results in frequency shifts of subcarriers which causes ICI at the FFT output.

OFDM is relatively more robust to timing errors than frequency errors. If the

[3]Uplink is the transmission directed from user equipment to base station

[4]Downlink is the transmission directed from base station to user equipment

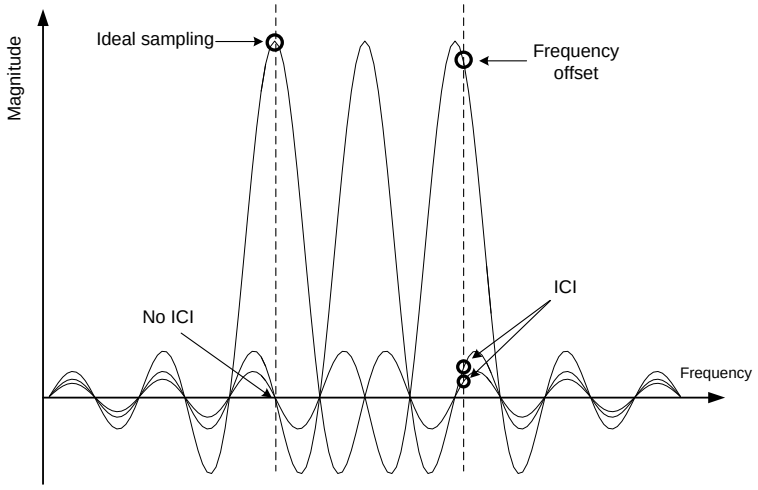

Figure 2.9 *Effect of intercarrier interference: frequency offset causes non-ideal sampling which induces interference from other subcarriers.*

CP is used as a guard period, the symbol timing offset may vary over an interval equal to CP, without causing interference (see Figure 2.6). Otherwise, orthogonality between CP-OFDM symbols is lost causing Inter Symbol Interference, which leads to degradation of OFDM system performance.

3. TIME DOMAIN WINDOWED CP-OFDM WAVEFORM

In this chapter, the fundamentals of Windowed CP-OFDM (W-OFDM) waveform is introduced. Time domain windowing is the popular low-complexity technique to lower side lobes of a CP-OFDM signal. It is implemented on top of basic CP-OFDM waveform introduced in Chapter 2. Overlap and Add processing is described to reduce errors caused by windowing in W-OFDM waveform processing. All additional parameters related to W-OFDM are explained in this chapter, used values are selected later in Chapter 5. Finally the mathematical expression of W-OFDM signal is introduced.

3.1 Windowed CP-OFDM

As discussed in Section 2.2.2, OFDM signal produces large side lobes in spectrum. The reason for that is rectangular pulse shape in time domain signal [28]. In frequency domain, CP-OFDM signal consist of a number of rectangular filtered QAM subcarriers resulting rather slow degrease of the out-of-band spectrum (see Figure 2.8). In Windowed CP-OFDM technique, N_{ws} (window size in samples) samples of time domain CP-OFDM pulse are windowed to suppress the symbol energy at the edge of the CP-OFDM symbols. The window duration is determined as $T_W = N_{ws}/F_S$, where F_S is the sampling frequency. Windowing transmitted OFDM symbols allows the amplitude to go smoothly to zero at the symbol boundaries leading to reduced discontinuity between symbols in time. This induces the spectrum of the transmitted signal to go down more rapidly [29]. Windowing loses some initial information, and thus, additional samples need to be inserted (along with cyclic prefix) to restore the received signal perfectly in receiver side processing. However, it should be noted that additional samples increases overhead of the symbol, which decreases the spectrum efficiency. *Overlap-and-add* (OLA) -processing (discussed further in section 3.2) is introduced together with W-OFDM to reduce the overhead caused by additional samples.

Weighted overlap-and-add (WOLA) technique, which is applied in W-OFDM

studied in this thesis, was already researched by 3GPP in [30]. Now WOLA has gained more interest due to its low-complex way of suppress side lobes of OFDM signal compared to filtering methods (discussed further in Chapter 4). Thus, it has been proposed for as a one potential candidate for 5G wireless communications [10]. Another interesting windowing technique - although the implementation complexity is increased - is to divide active bandwidth into several group, and then, different window sizes are applied to each group of subcarriers. Basically, subcarriers closer to the band edges leak power to side lobes outside of the allocated band, more than inner ones. Hence, it is beneficial to use longer window for edge group than for inner group(s) to improve spectral localization leading to reduced total inband Error Vector Magnitude (EVM). This method is called as *Edge Windowing* which is introduced in [31]. In this thesis, conventional single-windowing is applied in order to maintain the implementation complexity as low as possible i.e. only the one window size is used for each subcarrier due to its low-complexity. Edge Windowing and other multi-windowing schemes are potential topics for future research founded on this thesis.

3.2 Overlap and Add Processing

At Overlap-and-Add transmitter side processing, additional samples need to be added to reduce the interference induced by transmitted side (Tx) windowing. Thus, conventional CP-OFDM symbol is extended by N_{ext} samples, that is $T_{\text{ext}} = N_{\text{ext}} \times F_S$, in time units. This allows to use longer window sizes without increasing significantly receiver side Error Vector Magnitude (EVM) [1]. The total W-OFDM symbol becomes $T_{\text{W-OFDM}} = T_{\text{FFT}} + T_{\text{CP}} + T_{\text{ext}}$ in seconds and $N_{\text{W-OFDM}} = T_{\text{W-OFDM}}/F_S$ in samples. $N_{\text{ECP}} = N_{\text{CP}} + N_{\text{ext}}$ denotes *Extended Cyclic Prefix* (ECP) meaning that extended samples can be understood as a extension of traditional CP. This symbol is partially overlapped and summed on top of adjacent symbols as illustrated in Figure 3.1. Amount of overlap in time is denoted as T_{OL}. Overall W-OFDM transmitter side processing chain is illustrated in Figure 3.2 (a).

At receiver side, symbol of $N_{\text{W-OFDM}} = N_{\text{FFT}} + N_{\text{CP}} + N_{\text{ext}}$ samples is received. First, CP is removed, cutting the signal length to $N_{\text{FFT}} + N_{\text{ext}}$. Then receiver side windowing is performed to modify pulse shape of the received signal, which reduces the interference originated from adjacent channels by forcing the FFT input to be

[1] In telecommunications, Error Vector Magnitude (EVM) is a measure to quantify the performance of digital radio transmitter or receiver in the presence of impairments. It is defined as a vector difference between the ideal (transmitted) signal and measured (received) signal.

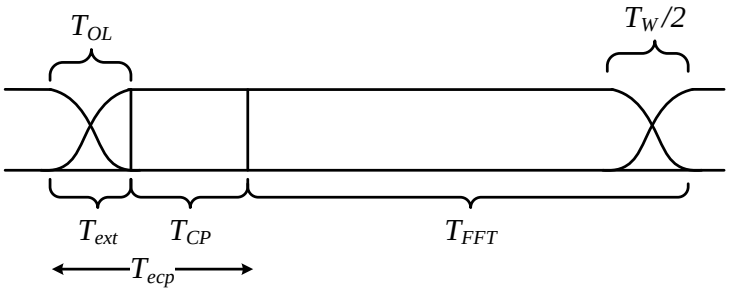

Figure 3.1 *Structure of W-OFDM symbol with adjacent symbols overlapping and related parameters.*

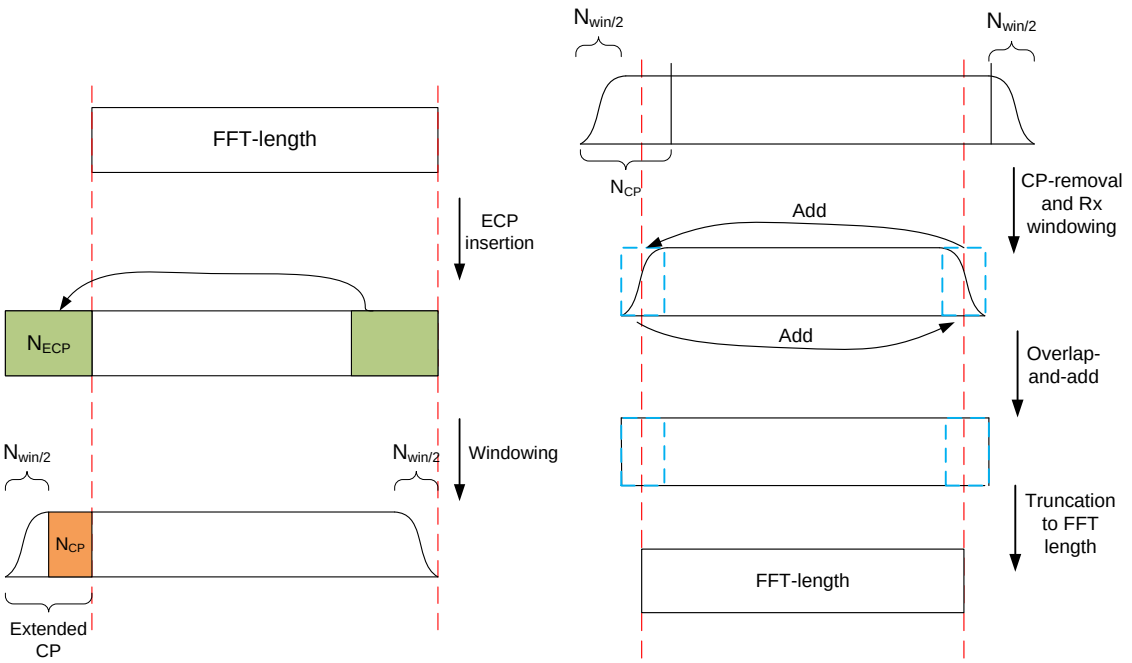

(a) W-OFDM transmitter processing. (b) W-OFDM receiver processing.

Figure 3.2 *Structure of W-OFDM (a) transmitter and (b) receiver processing and parameters.*

cyclic in nature. Overlap-and-add processing adds first N_{ws} samples part of the symbol to the end of the symbol and last N_{ws} samples to the beginning of the symbol. Lastly, signal is truncated back to initial size N_{FFT} having only information samples and no overhead. Receiver processing chain is demonstrated in Figure 3.2 (b).

Overlapping technique is introduced to deal with increased symbol time in W-OFDM. Additional samples (N_{ext}) needed for W-OFDM processing (recall section 3.1) increases the symbol time, and thus, the total transmission time increases cumu-

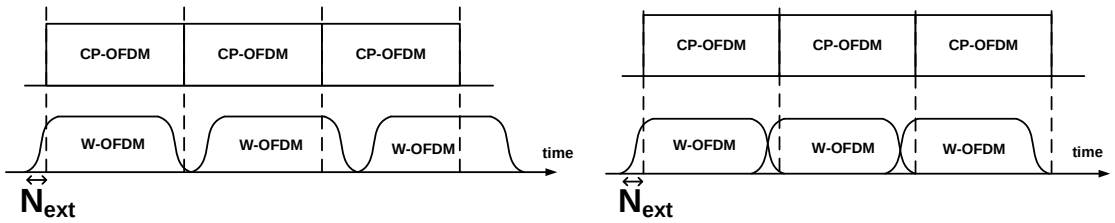

(a) W-OFDM symbols without overlap method. (b) Overlap method used to retain correct timing.

Figure 3.3 *Symbol timing of W-OFDM symbols (a) without and (b) with the overlapping method.*

latively related to number of symbols (see Figure 3.3 (a)). In W-OFDM prosessing, two consecutive symbols are allowed to interfere in windowed interval $T_W/2$ in both ends, as shown in Figure 3.1. This decreases the time losses due to additional samples and initial transmission time can be preserved by overlapping symbols according to number of extended samples N_{ext}. This is illustrated in Figure 3.3 (b), in which a time shift of $N_{\text{ext}/2}$ would align W-OFDM signals perfectly.

3.3 Window function

In this thesis, commonly used window function, *Raised Cosine* (RC) window [29], is used as a W-OFDM window function. It is defined as

$$w(t) = \begin{cases} 1/2 + 1/2\cos\left(\pi + \frac{\pi t}{\alpha T_{\text{W-OFDM}}}\right) & \text{if } 0 \leq t < \alpha T_{\text{W-OFDM}} \\ 1 & \text{if } \alpha T_{\text{W-OFDM}} \leq t \leq (1-\alpha) T_{\text{W-OFDM}} \\ 1/2 + 1/2\cos\left(\pi + \pi \frac{T_{\text{W-OFDM}} - t}{\alpha T_{\text{W-OFDM}}}\right) & \text{if } (1-\alpha) T_{\text{W-OFDM}} < t \leq T_{\text{W-OFDM}} \\ 0 & \text{otherwise,} \end{cases} \tag{3.1}$$

where α defines the roll-off factor of the window. Roll-off factor determines the window size (i.e. transition band) $T_W = \alpha \times T_{\text{W-OFDM}}$ indicating how fast RC window goes to zero. In frequency domain, higher roll-off factor results to signal spectrum go down faster at the edge of the active band. From Figure 3.4, the effect of windowing can be observed. Roll-off factor equal to zero corresponds to conventional CP-OFDM signal without any windowing. Higher the roll-off factor is (i.e. the transition band is larger), better the spectral localization of signal is. This leads to reduced side lobe powers as depicted in 3.4, where 600 active LTE

subcarriers (corresponds to a LTE-like 9 MHz bandwidth, explained later in Section 5.2.1) carrying four W-OFDM symbols with $N_{\mathrm{CP}} = 72$ is plotted in cases of different roll-off factors.

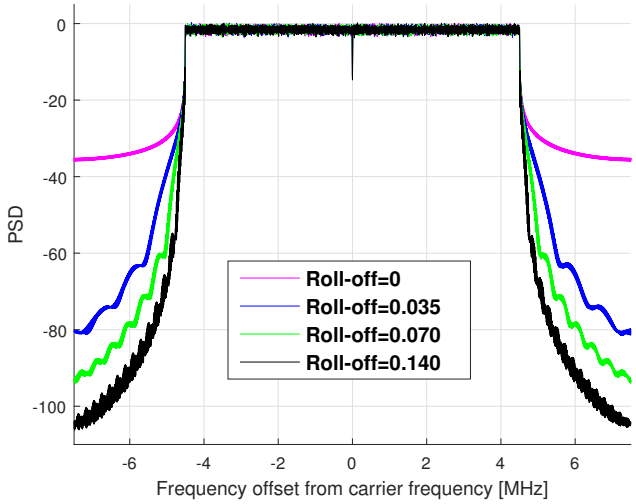

Figure 3.4 *Effect of roll-off factor in W-OFDM signal. Roll-off = 0 corresponds to a conventional CP-OFDM singal.*

In W-OFDM processing, transmitted CP-OFDM signal is multiplied by a window function to achieve more suitable pulse shape (see (2.3)). The total transmitted W-OFDM signal, where extended CP is also considered, is defined as

$$y(t - T_{\mathrm{ext}}/2) = \sum_{n=-\infty}^{\infty} \left[\sum_{k=0}^{N-1} s_k e^{(j2\pi k \frac{t - nT_u - T_{\mathrm{CP}} - T_{\mathrm{ext}}}{T_u})} \right] w(\frac{t - nT_u}{T_u}), \tag{3.2}$$

where T_u is the symbol timing and $w(t)$ is the used time domain window described in (3.1). The timing of the generated signal $y(t)$ in (3.2) is shifted by $T_{\mathrm{ext}}/2$ to align the transmitted signal with the original CP-OFDM, as shown in Figure 3.3.

It is noted that window cannot be chosen in an arbitrary way. Larger window suppresses side lobes more effectively, but available time resources need to be considered. Symbol is extended according to window size (see Section 3.1) and symbol time increases relatively to window size. Hence, there is always a trade-off between window size and overhead caused by additional samples, which is discussed in Section 3.2. It is common to choose window size as a fraction of used CP length, which is followed in the window size selection in Section 5.2.2. From now on, only window size is considered instead of roll-off factor, as one determines the other parameter unambiguously as a function of W-OFDM symbol time $T_{\text{W-OFDM}}$.

4. FAST CONVOLUTION BASED FILTERED OFDM WAVEFORM

In this chapter, the main focus is to introduce *Fast Convolution based Filtered OFDM* as a other potential method to reduce high side lobes of CP-OFDM signal. First, basics of filtered CP-OFDM (F-OFDM) approach is explained with a few example waveforms which has gain more interest in 5G development. Then, FC-F-OFDM is presented as a our proposal for a 5G waveform candidate.

4.1 Filtered OFDM scheme

To improve spectral localization of the conventional OFDM, filtering is introduced as a one potential method in order to efficiently reduce the out-of-band emissions. It is an important advantage to have OFDM as its core waveform, and thus, to enjoy desirable features of OFDM and applications of existing OFDM-based designs [32]. This popular filtering based method is generally called as *Filtered OFDM* (F-OFDM) [33].

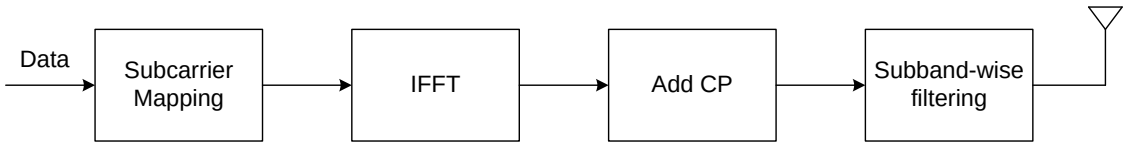

Figure 4.1 *Basic transmitter processing chain of F-OFDM techniques.*

In the basic F-OFDM implementation, subband-wise filtering is added after normal CP-OFDM processing in order to reduce side lobes of the transmitted signal. Subband size can be chosen according to system requirements and filtering is performed per each subband. Fullband filtering scheme is a special F-OFDM case, where the subband corresponds to the maximum number of active subcarriers inside a channel bandwidth. Plain F-OFDM processing chain is demonstrated in Figure 4.1.

As the available unlicensed bands are a scarce resource, the spectrum used for transmission will be more often non-contiguous as demonstrated in Figure 4.2. That

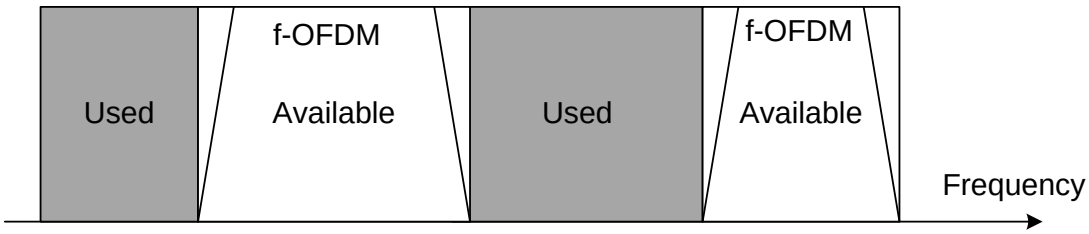

Figure 4.2 *Utilization of non-contiguous spectrum.*

leads to challenging implementation of the filter design, as it needs to be designed specifically for each available chunk of spectrum. That is also a big challenge when spectrum availability changes dynamically and the size of a optimal filter varies in time [33].

4.1.1 Relevant Filtered OFDM techniques for 5G systems

As mentioned earlier, the filtering is generally performed in several parts i.e. subbands. One popular filtering scheme is so called *Filter Bank Multicarrier* (FBMC), which is designed for maximum bandwidth efficiency. FCFB techniques uses filtering on a per subchannel and typically are used only with offset QAM (OQAM). That is because the orthogonality of subchannels can not be maintained with complex data symbols (as in QAM), which leads to problems in channel estimation and in MIMO schenarios [18]. The subchannel filters are generally very narrow in frequency requiring rather long filter lengths, which is major drawback in FBMC systems. It is notable that most of the advantages of FBMC originate from the fact that, by design, the nonadjacent subchannels in this modulation are separated almost perfectly through a bank of well-designed filters, which increases the complexity [18]. Nevertheless, in case of FBMC, the available spectrum fragments can be divided in the blocks of contiguous subchannels. Different types of services can be accommodated in different subchannels with the most suitable waveform and numerology, which leads to an improved spectral utilization compared to conventional CP-OFDM waveform [34].

Other filtered OFDM scheme, which has gained a huge interest in 5G development, is called here as WinSinc-F-OFDM and is introduced in [34]. The basic principle is to use Hann windowed sinc-function as a filter, where the sinc-function is defined based on the used allocation bandwidth. With subband-based band splitting filtering - meaning that the used bandwidth is split into several subbands - independent OFDM systems (and possibly other waveforms) are closely contained

in the assigned bandwidth. In this way, it is possible to overcome the drawbacks of OFDM whilst retaining the advantages of it [34]. This waveform is denoted as WinSinc-F-OFDM in Figure 4.3.

Universal Filtered OFDM (UF-OFDM), sometimes also referred as *Universal Filtered Multicarrier* (UFMC) is a generalization of two previously represented techniques. While FBMC filters narrow subchannels individually, UF-OFDM filters the signal on blocks of subcarriers. That method is called as block-wise filtering, which brings additional flexibility and may be used to avoid the main FBMC drawbacks. Transition band of the filter is wider, that is, shorter filter length in time. Shorter filter lengths makes it applicable for short bursts communications. That is beneficial feature for future 5G wireless scenarios, like small packets, low latency, energy-efficient transmission and fast *Time Division Duplexing* (TDD) switching, which is why UF-OFDM is a one proposed waveform candidate for 5G wireless communication systems [35]. UF-OFDM processing is typically associated with zero prefix, but it can be equally well used with cyclic prefix. Comparison between CP-OFDM, FC-F-OFDM and UFMC is done in [36], showing the UF-OFDM superiority especially in short-burst communication. [4, 37]

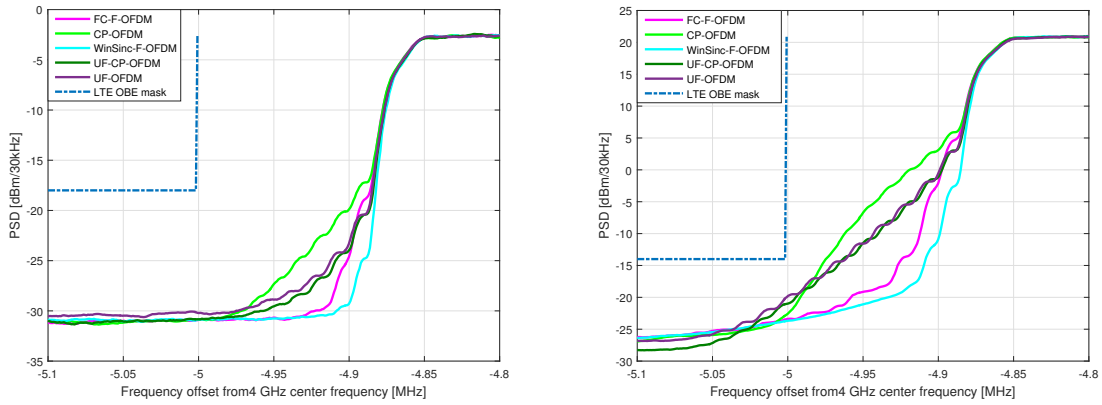

(a) Uplink 54 PRB allocation.

(b) Downlink 54 PRB allocation.

Figure 4.3 *Spectral localization of different F-OFDM techniques with 54 PRB allocation zoomed to the left side of the 10 MHz LTE channel in (a) UL and (b) DL.*

Spectral localization, zoomed to the 10 MHz LTE channels left edge, is shown in Figure 4.3 for the most interesting filtered OFDM waveforms. 54 *Physical Resource Block* (PRB) allocation allocation is used, which is interesting for 5G research in order to increase spectral efficiency (explained in more details in Chapter 5). Dolph-Chebyshev Finite Impulse Response (FIR) filter is used in UF-OFDM, which

is evaluated with zero prefix and CP, denoted as UF-OFDM and UF-CP-OFDM respectively in Figure 4.3. LTE like channel filtered CP-OFDM is denoted here as CP-OFDM. FC-F-OFDM waveform, which is discussed thoroughly in Section 4.2, is already considered here as it is our proposal for the best filtered OFDM scheme. *Modulation and Coding Scheme* (MCS) 64-QAM, $R = 3/4$, where R denotes coding rate, and input backoff (explained in Section 5.4) of 4.8 dB is used. 30 kHz measurement bandwidth is used to define the LTE out-of-band emission (OBE) mask, which defines the limit for signals power leakage. LTE OBE masks and other parameters are introduced later in Chapter 5.

From Figure 4.3, it can noticed that all filtered-OFDM have rather similar spectra. While WinSinc-F-OFDM having slightly lower side lobe than FC-F-OFDM, the UFMC waveforms with CP and zero prefix have the worst performance in terms of power leakage. It should be emphasized that each of these filtered OFDM waveforms have relatively low side lobe, as none of them are exceeding the LTE OBE mask with 54 PRB allocation. The current LTE is specified to use 50 PRBs in 10 MHz channel meaning that all these filtering schemes allow to support larger bandwidth allocation than currently supported in LTE.

Additionally, to utilize F-OFDM waveforms effectively, proper filter design is needed. The baseline of the filter design is to consider the tradeoff between the time- and frequency characteristics together with implementation complexity [34]. The filter design is out of the scope in this thesis, but is a potential topic for future research founded on this thesis.

4.2 Fast Convolution Based Filtered OFDM

Other efficient variation of F-OFDM technique is a *Fast Convolution based Filtered OFDM* (FC-F-OFDM) scheme, which is described thoroughly in this section. It is a special implementation for multirate filter banks which are based on fast-convolution (FC). The basic idea is to use frequency domain multiplications for high-order filter implementation. This is performed after FFT operations for input sequence and filter impulse response [38]. The time domain signal is eventually obtained by using IFFT, just like in CP-OFDM. Overlapped block processing together with FFT-IFFT pair offer a straightforward way to adjust the frequency domain characteristics of the filters.

4.2.1 Description of Fast Convolution Filter Bank Schemes

The structure of the FC-F-OFDM synthesis filter bank (SFB), which is used in FC-F-OFDM transmitter side, is shown in Figure 4.4. Several incoming low-rate narrowband signals $\mathbf{x}_m$ for $m = 0, 1, 2, ..., M-1$ are combined into single wideband signal $\mathbf{y}$, following the frequency division multiplexing principle. These narrowband input signals can be easily adjusted in terms of bandwidths, center frequencies, frequency responses, and output sampling rates [38]. The dual structure can be used on the receiver side as an analysis filter band (AFB) for splitting the incoming high-rate, wideband signal into several narrowband signals [39], which is demonstrated in Figure 4.5. The cascade of SFB and AFB is often called as transmultiplexer.

SFB first segments each of the M incoming signals into overlapping blocks of length L_m. Then L_m-sized FFT is used to transform input blocks to frequency-domain. Here, the frequency domain window is obtained by optimizing the transition band weights directly in frequency domain as they consist of two symmetric transition bandwidths (TBWs). In the used frequency domain windows, passband is ones and stopband is zeros. Hence, only the transition band weights used for with all different subband widths need to be stored to the device, which requires low memory capacity [40]. Weighted signals are eventually combined and converted back to time-domain using N-length IFFT. Overlap-and-save (OLS) principle is utilized to concatenate obtained time-domain output blocks [41, 42]. Receiver side OLS processing is illustrated in Figure 4.6.

In FC-F-OFDM, sampling rate conversion is included by factors

$$I_m = N/L_m = N_{NO}/L_{S,m}, \tag{4.1}$$

where m is the subband index. $L_{S,m}$ and N_{NO} are the number of non-overlapping input and output samples, respectively. The sampling rate conversion factor I_m is determined by the IFFT size L_m, which determines the maximum number of non-zero frequency bins and it can be configured for each subband individually.

In the AFB case, it is assumed that the forward transform length is larger than the inverse transform lengths, which means the above process reduces the sampling rate (shown in Figure 4.6) of the subband by factors of

$$H_m = N/\bar{L}_m = N_{NO}/\bar{L}_{S,m}, \tag{4.2}$$

where IFFT lengths of AFB side are denoted by $\bar{L}_{S,m}$. Long transform length N is assumed to be equal length in both SFB and AFB side.

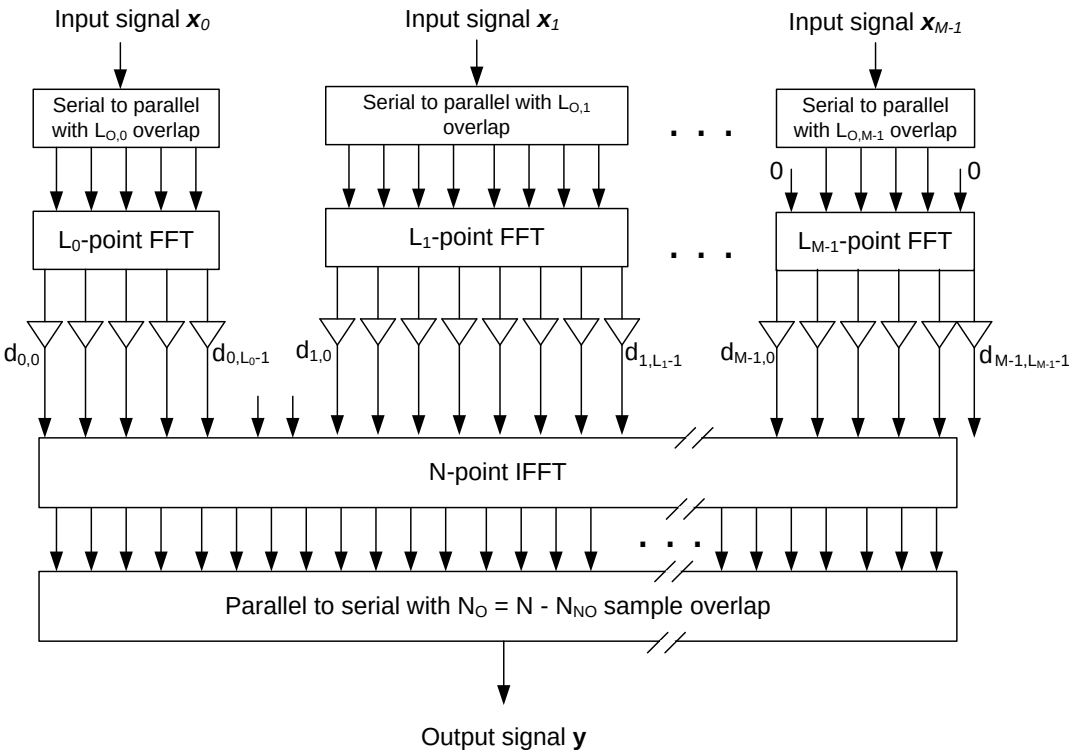

***Figure** 4.4 Fast convolution based synthesis filter bank for FC-F-OFDM transmitter.*

4.2.2 Matrix model for Fast Convolution Filter Bank Analysis

The FC-F-OFDM processing is performed by using matrix notation. Transmitter side (i.e. synthesis filter bank) block processing of mth subband signal $\mathbf{x}_m$ can be represented as

$$\mathbf{w}_m = \mathbf{F}_m \mathbf{x}_m, \tag{4.3}$$

where $\mathbf{F}_m$ is the block diagonal matrix of the form

$$\mathbf{F}_m = diag(\mathbf{F}_{m,0}, \mathbf{F}_{m,1}, ..., \mathbf{F}_{m,R_m-1}) = \begin{bmatrix} \mathbf{F}_{m,0} & & & \\ & \mathbf{F}_{m,1} & \mathbf{0} & \\ & & \cdot & \\ & \mathbf{0} & & \cdot \\ & & & \mathbf{F}_{m,R_1} \end{bmatrix} \tag{4.4}$$

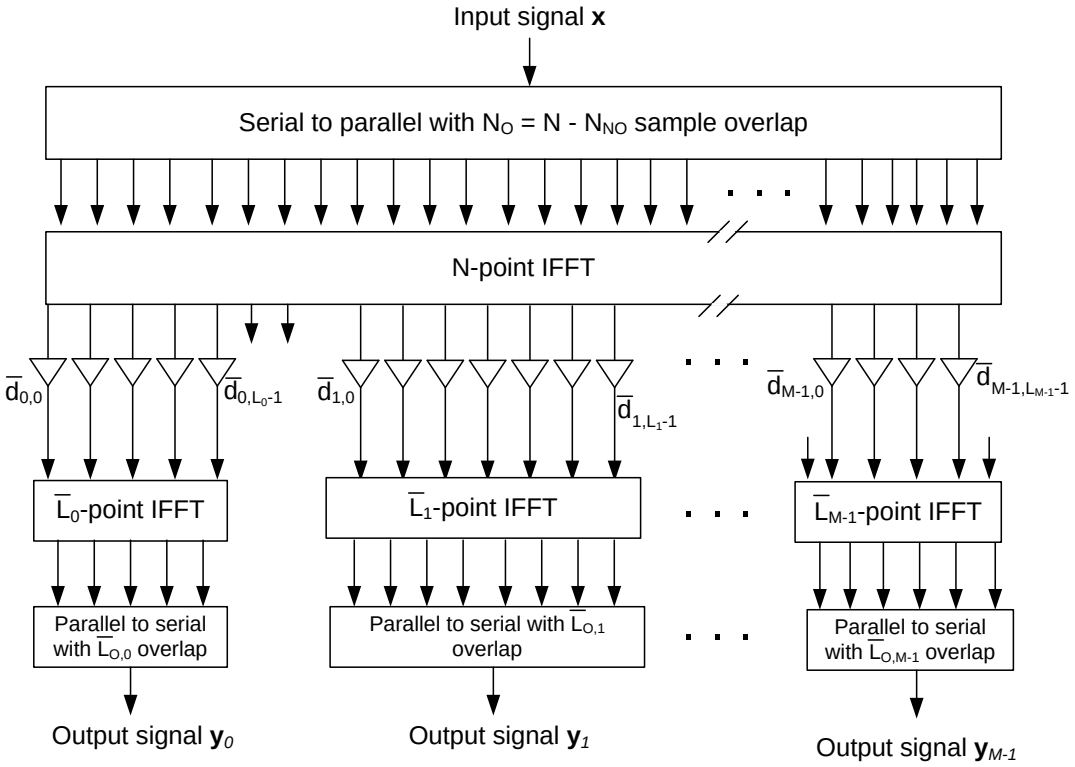

Figure 4.5 *Fast convolution based analysis filter bank for FC-F-OFDM receiver.*

having R_m processing blocks [40]. Overlapping factor for the OLS processing determines the dimensions of the $\mathbf{F}_{m,r}$. Overlapping factor λ is defined as

$$\lambda = 1 - L_{S,m}/L_m = 1 - N_{NO}/N, \tag{4.5}$$

where $L_{S,m}$ and N_{NO} are the number of non-overlapping input and output samples, respectively.

The multirate version of the fast-convolution synthesis filter bank can be now defined using block processing by decomposing the $\mathbf{F}_{m,r}$'s as the following $N_{NO} \times L_m$ matrix

$$\mathbf{F}_{m,r} = \mathbf{S}_N \mathbf{W}_N^{-1} \mathbf{M}_{m,r} \mathbf{D}_m \mathbf{P}_{L_m}^{(L_m/2)} \mathbf{W}_{L_m}, \tag{4.6}$$

where $\mathbf{W}_{L_m}$ and $\mathbf{W}_N^{-1}$ are the $L_m \times L_m$ FFT matrix and $N \times N$ IFFT matrix, respectively. The FFT shift matrix $\mathbf{P}_{L_m}^{(L_m/2)}$ is circulant permutation matrix obtained by cyclically left shifting the $L_m \times L_m$ identity matrix by $L_m/2$ positions [40]. $\mathbf{D}_m$ is the diagonal matrix of size $L_m \times L_m$ containing the frequency-domain window weights for each subband m on its diagonal. $\mathbf{M}_{m,r}$ and $\mathbf{S}_N$ are the frequency-domain

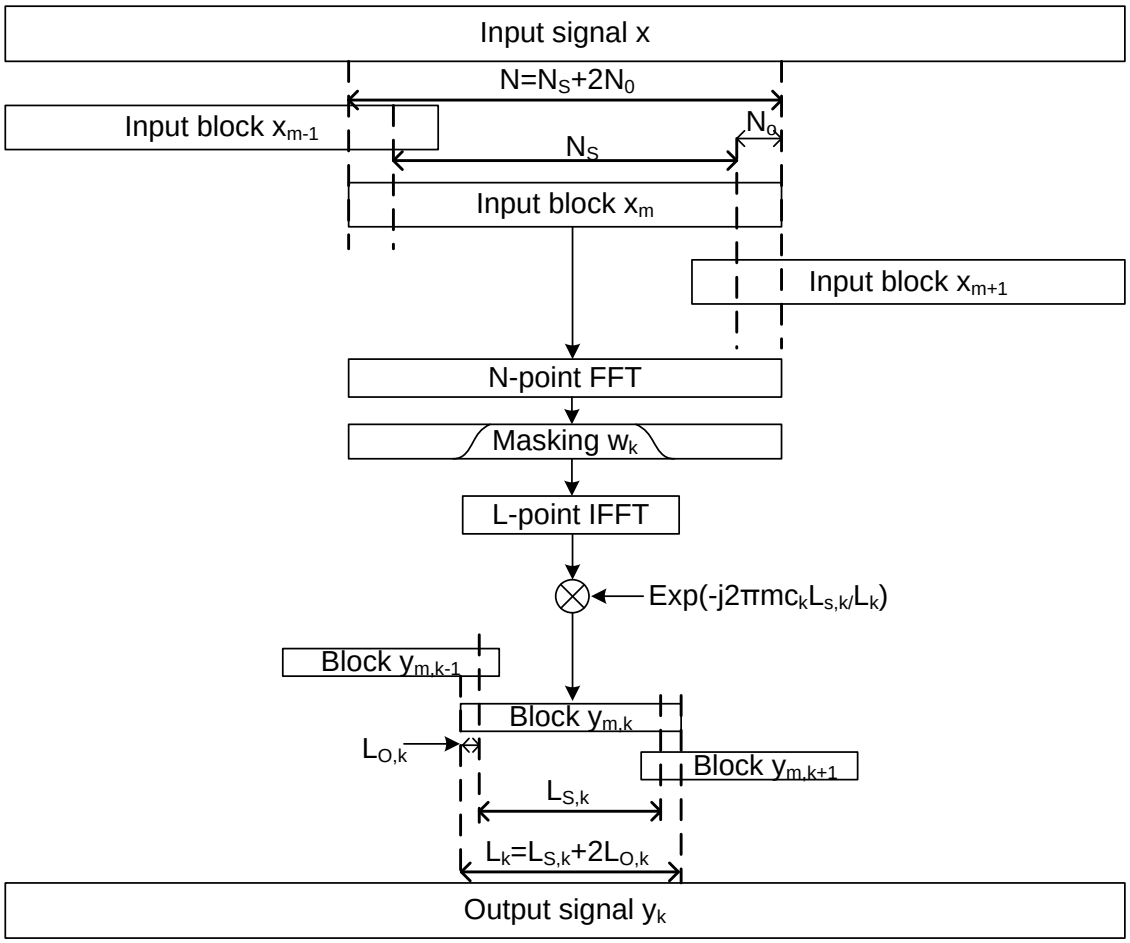

Figure 4.6 *Overlap and save processing used at FC-F-OFDM receiver.*

mapping and time-domain selection matrices, respectively. The $N \times L_m$ frequency-domain mapping matrix maps L_m frequency-domain bins of the input signal to frequency-domain bins $(c_m - \lceil L_m/2 \rceil + l)_N$ for $l = 0, 1, ..., L_m - 1$ of output signal [40]. Here c_m is the center bin of the subband m and $(\cdot)_N$ denotes the modulo-N operation. It should be noted that this matrix rotates each block by phase of

$$\theta_m(r) = \exp(j2\pi r\theta_m) \quad \text{with} \quad \theta_m = c_m L_{\mathrm{S},m}/L_m, \tag{4.7}$$

in order to maintain the phase continuity between the consecutive overlapping processing blocks [43]. The $N_\mathrm{S} \times N$ selection matrix $\mathbf{S}_N$ selects the desired N_S output samples from the inverse transformed signal in order that OLS processing is applied.

Simliar to SFB, the corresponding analysis sub-block matrix of size $\bar{L}_{\mathrm{S},m} \times N$

used in the FC-F-OFDM receiver, can be decomposed as

$$\mathbf{G}_{m,r} = \mathbf{S}_{\bar{L}_m} \mathbf{W}_{\bar{L}_m}^{-1} \mathbf{P}_N^{(N/2)} \mathbf{D}_m \mathbf{M}_{m,r}^T \mathbf{W}_N, \tag{4.8}$$

where $\mathbf{P}_N^{(N/2)}$ is the inverse Fourier-shift matrix and the $\mathbf{S}_{\bar{L}_m}$ is $\bar{L}_{\mathrm{S},m} \times \bar{L}_m$ selection matrix, which selects the desired $\bar{L}_{\mathrm{S},m}$ output samples from the inverse transformed output signal.

4.2.3 FC Filtered OFDM waveform

In this thesis, performance of the FC-F-OFDM is evaluated as a comparison for LTE like channel filtered CP-OFDM technique used in current LTE-technology. FC filter banks are applied for resource block group wise filtering while utilizing normal CP-OFDM waveform. It is a conventional method for scenarios, in which the different service exploits different resource blocks. In addition, it is possible to parametrize users according to their traffic requirements. That is usually the case in cellular uplink case, where users run different applications demanding different throughput. In FC-F-OFDM, this can be implemented by allocating various subcarrier spacings or CP lengths, also depending on the channel conditions, and thus, resource block groups of different users can be separated by using FC-based filter banks [40].

Other remarkable advantage of FC-F-OFDM processing is the ease to adjust filtering bandwidth for each physical resource block group independently. This is very useful in PRB-filtered OFDM because it is not needed to realize filter transition bands and guardbands between equally parametrized synchronous PRBs. In the extreme case, the group of filtered PRBs could cover the full carrier bandwidth, and FC processing would implement tight channelization filtering for the whole carrier. [40]

5. SIMULATION ASSUMPTIONS

To compare enhanced CP-OFDM waveforms described earlier in Chapters 3 and 4, several simulations are executed. In this chapter, the simulation tool used in this thesis is introduced. First, evaluated waveforms are listed and waveform related parametrization are chosen and explained. Then, channel models and PA models, which have important role to simulation results, are described. Finally, the complexity of the waveforms are compared as it is an important metric in addition to transmitter performance results and overall link performance results studied in Chapters 6 and 7, respectively.

5.1 Evaluated waveforms

In technical report TR 38.802 [13] it is given that the baseline waveform for 5G-NR physical layer is CP-OFDM. Therefore, waveforms examined in this thesis are based on windowing or filtering CP-OFDM signals described in Chapters 3 and 4, respectively. LTE like channel filtering is used as a reference in UL and DL results. In addition, *DFT-spread-OFDM* (DFTs-OFDM) waveform is considered in UL evaluations and is introduced in Section 5.1.3. It was agreed that DFTs-OFDM is to be supported in uplink coverage limited scenarios in [13].

5.1.1 LTE like CP-OFDM

As was discussed in Chapter 2, the spectrum of an CP-OFDM signal decays rather slowly outside of the transmission bandwidth. Since the transmitted signal for LTE occupies 90% of the channel bandwidth (explained in more details in Section 5.2.1), it is not possible to directly meet the unwanted emission limits with pure CP-OFDM signal. However, the techniques used for achieving the transmitter requirements are, not specified or mandated in LTE specifications [15].

In a modern LTE basestation, the channel filtering is typically applied in addition to the basic CP-OFDM waveform to achieve LTE OBE masks defined later in Section 5.2. In this thesis, FIR channel filter is used. As the fullband filtering scheme filters the whole channel, the channel filter has to be defined for each fullband allocation

size individually. Therefore, if the bandwidth efficiency is increased by allocating more resource blocks, the channel filter length should be larger. It should be noted that inside a LTE channel the allocation size of the signal does not effect to the filter length, only the defined maximum allocation does. From now on, LTE-like channel filtered CP-OFDM is denoted as CP-OFDM for simpler presentation. It is used as a reference in the results in Chapters 6 and 7 to observe improvements compared against the current LTE solution.

5.1.2 Enhanced OFDM waveforms

The FC-F-OFDM and W-OFDM schemes described in Chapters 3 4 are compared against the current LTE solutions with parametrization described later in Section 5.2. These waveforms are relevant for 5G research, as the 5G NR waveform consist of CP-OFDM with some form of filtering or windowing [9, 13].

FC-F-OFDM and W-OFDM are evaluated in both, uplink and downlink transmission schemes. Even though the current LTE system have different waveforms for UL and DL, the target is to find waveform, which can overcome the challenges of both transmission directions. In technical report TR 38.802 it has been already accepted, that CP-OFDM is the baseline waveform for below 40 GHz communications in both DL and UL.

5.1.3 DFTs-OFDM

As discussed earlier in Section 2.2.2, high peak-to-average ratio is one of the main problems in OFDM. This leads to complex PA designs, because it is difficult to reach the required linearity with reasonable electrical efficiency [44]. This is problematic especially in UL transmission, in which the user equipments are tightly restricted in size to retain comfortable usability. Therefore, single carrier transmission schemes are found important when considering hand-held devices [45]. In LTE, using only DFTs-OFDM in UL leads to a significantly different PA implementation than in downlink, which utilizes multi-carrier transmission scheme.

To deal with challenging PA design conditions of multicarrier OFDM, the LTE uplink transmission scheme is based on single carrier FDMA, more specifically on DFTs-OFDM [46]. DFTs-OFDM has relatively smaller variations in the instantaneous power of the transmitted signal due to single carrier property [15]. The basic principle in DFTs-OFDM is illustrated in Figure 5.1. First, a block of M modulation symbols are applied to a size-M FFT. Then, the output of the FFT is mapped to allocated subcarriers and rest unused subcarriers are set to zero. This is fed into a

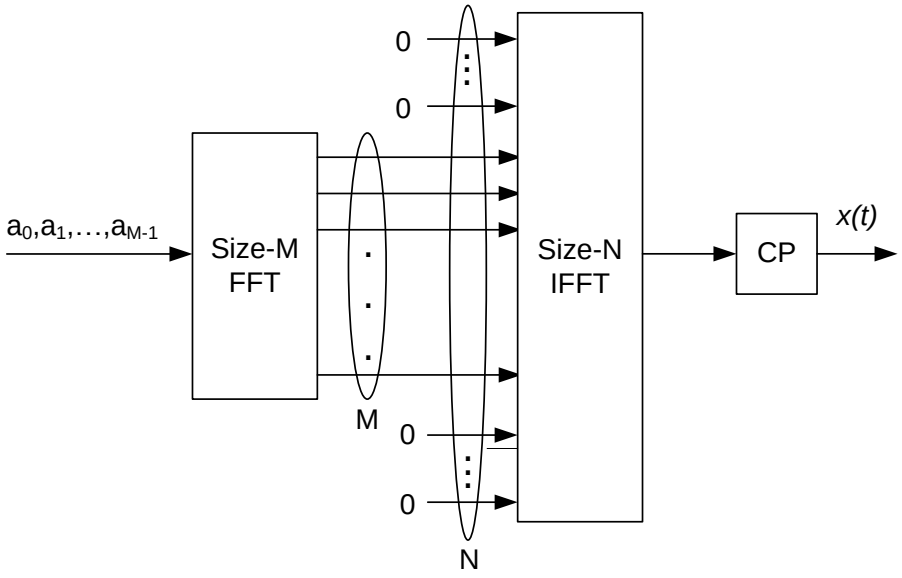

Figure 5.1 *DFT-s OFDM transmitter processing used in LTE uplink.*

OFDM modulator which is implemented as a size-N IFFT ($N > M$). Typically N is selected as $N = 2^n$ for some integer n to allow for the IFFT to be implemented by means of computationally efficient radix-2 IFFT processing [15]. Also similar to basic CP-OFDM, cyclic prefix is used to deal with multipath propagation.

In the current LTE systems, DFTs-OFDM is used in uplink, which requires filtering or windowing to achieve the uplink emission masks defined in Section 5.2. Hence, LTE like channel filtering described in Section 5.1.1, is used also with DFTs-OFDM. That LTE like DFTs-OFDM waveform is evaluated as a reference waveform in all uplink simulation cases further in Chapters 6 and 7. It should be noted that DFTs-OFDM is suitable only for LTE uplink [15], and thus, is not included in downlink simulation results. New proposed waveforms should obtain similar link level performance result than DFTs-OFDM to be concerned as a potential 5G new radio waveforms. Furthermore it is defined in TR 38.803 [47] that in 5G NR DFTs-OFDM is supported only in UL in coverage limited scenarios and single stream transmission. It also states that all *User Equipments* (UEs) have to support DFTs-OFDM.

5.2 Parametrization

In this section, the baseline LTE parametrization is represented for a 10 MHz channel bandwidth. In addition to basic LTE like CP-OFDM parameters (presented in Table 5.1), some waveform specific parameters are introduced along with filtering and windowing techniques. Additional parameters concerning W-OFDM and FC-

F-OFDM are defined and explained later in Sections 5.2.2 and 5.2.3, respectively, after the LTE parametrization is familiarized.

5.2.1 LTE parametrization

The LTE like CP-OFDM signal follows the LTE signal numerology for 10 MHz band. The only exception is that only a single CP length is used for all symbols for simplicity. All LTE related key parameters for 10 MHz channel bandwidth are listed in Table 5.1 [46]. It is notable that a guard period of 72 samples ($N_{GP} = 72$) is added to each subframe. That allows rising and falling transients caused by filtering and windowing in FC-F-OFDM and W-OFDM, respectively.

Table 5.1 *Physical layer parametrization for LTE like CP-OFDM.*

Bandwidth (B)	10 MHz
Sampling rate (F_S)	15.36 MHz
FFT size (N_{FFT})	1024
CP length (N_{CP})	72
Guard period length (N_{GP})	72
Subcarrier spacing (ΔF)	15 kHz
Number of PRBs (N_{PRB})	50
Number of SCs per PRB ($N_{\mathrm{SC/PRB}}$)	12
Number of active SCs (N_{ACT})	600
Number of OFDM symbols per subframe (N_{SYM})	14

Channel bandwidth is selected here to be 10 MHz, which is one of the defined channel bandwidths in the LTE system [15, 46]. Sampling rate (F_S), FFT size (N_{FFT}), CP length (N_{CP}) and maximum number of PRBs (N_{PRB}) are defined explicitly for 10 MHz channel (see Table 5.1). In LTE system, active subcarriers are grouped into physical resource blocks consisting of 12 consecutive subcarriers $N_{\mathrm{SC/PRB}} = 12$ in the frequency domain. One subframe consist of 14 CP-OFDM symbols ($N_{\mathrm{SYM}} = 14$) and a guard period is added to each subframe.

When considering power leakage to adjacent channels, LTE out-of-band emission masks are defined for LTE system. Waveforms must achieve these emission mask, which are defined for base station (i.e. downlink) in [48] and for user equipment (i.e. uplink) in [49], which are demonstrated later in Figures 6.1 (a) and 6.1 (b), respectively.

5.2.2 W-OFDM parametrization

For W-OFDM, window size should be chosen beneficially. Generally, window sizes (N_{ws}) are chosen as a fraction of used CP length (N_{CP}) in symbols. Here, window sizes of $N_{\mathrm{CP}/2}$, N_{CP}, $2 \times N_{\mathrm{CP}}$ are compared to find the best option in terms of link level *Block Error Rate* (BLER) [1] performance. In our simulations, CP length equals to 72 samples (see Table 5.1) meaning that examined window sizes are 36, 72 and 144 samples. Effect of window size as a function of BLER in DL is shown in Figure 5.2 with high MCS scenario (64-QAM, $R = 3/4$), which is used in most simulations later in Chapter 7. Channel model TDL-C-1000 is used (introduced in Section 5.3), as it has longer delay spread, and thus, differences between window sizes are clearer.

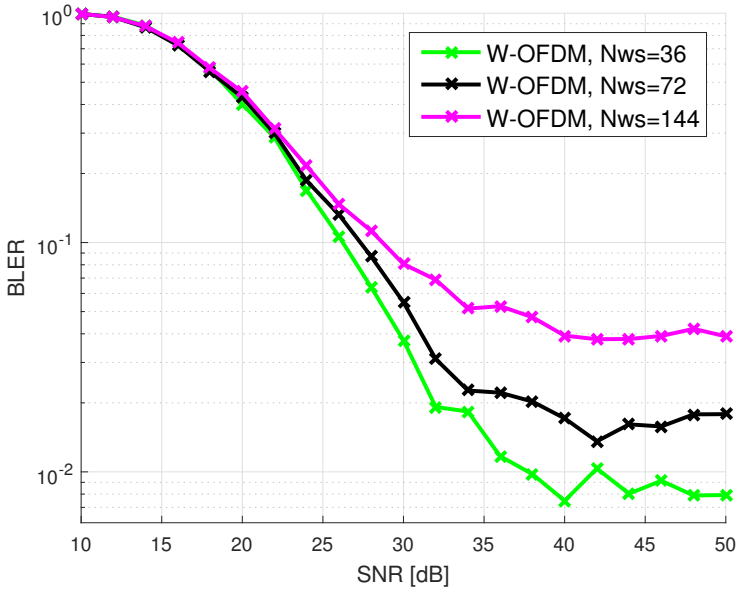

Figure 5.2 *Effect of W-OFDM window size in terms of BLER performance in TDL-C-1000 channel.*

From Figure 5.2, it can be seen that the shortest window size achieved the lowest BLER value and is the only one to achieve under 1% BLER inside the SNR range of 10...50 dB. Therefore, window size of $N_{ws} = N_{\mathrm{CP}/2} = 36$ samples is an intuitive choice for simulations. In addition to the best BLER performance, the complexity is the lowest as the complexity of windowing increases when window size in increased (evaluated later in Section 6.4). The drawback of short window is the poorer side lobe suppression feature as seen in Figure 3.4. However, the trade-off between

[1] BLER is one way to measure error rate of the transmission. It is defined as a ratio of the number of erroneous blocks to the total number of blocks received.

parameters should be done and here interference free link performance is given a higher importance.

5.2.3 FC-F-OFDM parametrization

Similar comparison is done for the frequency domain window used in FC-F-OFDM processing as for W-OFDM window size in Section 5.2.2. Typically TBWs of 1 to 7 FFT bins are used. Wider transition bands reduce the interference on top of edge most SCs while reducing the spectral containment. Increasing the TBW in frequency also reduces the effective impulse responses in time domain. The complexity increase caused by wider transition bands is minimal compared to overall FC-F-OFDM complexity as discussed in Section 6.4.1. Effect of transition bandwidth in terms of link level BLER performance is shown in Figure 5.3, when TDL-C-300 channel model (introduced in Section 5.3) is used with high MCS scheme (256-QAM and $R = 4/5$) and downlink transmission scenario is assumed.

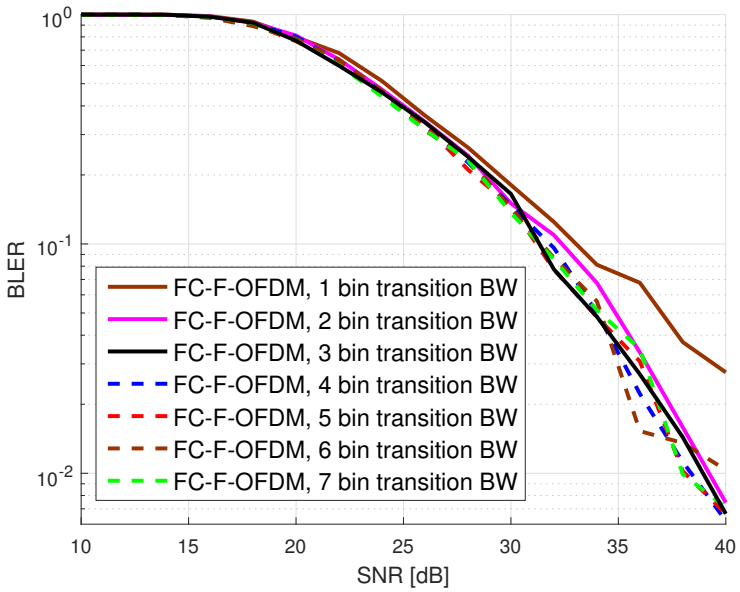

Figure 5.3 *Effect of FC-F-OFDM frequency domain window transition bandwidths in terms of EVM performance.*

Transition bandwidth should be chosen so that 256-QAM can be used without significant performance degradation. The target is to choose narrow transition bandwidth, which is beneficial in the presence of interfering signals (interference scenarios are described in more details later in Chapter 7). From Figure 5.3 it is notable that TBW of 1 frequency bin results in significantly higher BLER value especially in

higher SNR values. Increasing TBW larger than 3 bins (solid black line in Figure 5.3) does not gain notable improvement in terms of link level BLER performance. Hence, 3 bin transition bandwidth is considered here as a proper trade-off between filtering properties and side lobe suppression feature and is used in FC-F-OFDM simulations. In addition, 3 bin TBW can be used also for 54 PRB fullband filter, which is relevant and interesting for 5G NR [50].

Another important parameter for FC-F-OFDM is the overlapping factor as discussed in Chapter 4. Overlapping factor $\lambda = 1/2$ is selected for overlap-and-save method in FC processing to gain performance improvement without increasing implementation complexity too much. Higher overlapping factor would result in better performance but the complexity is also increased, which is stated later in Section 6.4.1.

5.3 channel models

For link simulations, evaluated waveforms are run through a channel model. Different channel models can be used in order to mimic various channel conditions in real life wireless communications. In this thesis, the channel models are described in terms of *Tapped Delay Line* (TDL). TDL model represents the channel by a delay line with N taps. As an example of TDL, 4-tap model ($N = 4$) is illustrated in Figure 5.4. That represents the impulse response of a multipath channel by a discrete number of impulses as follows:

$$h(\tau) = \sum_{i=1}^{N} c_i \delta(\tau - \tau_i), \tag{5.1}$$

where c_i and τ_i are coefficients and delays of the multipath components, respectively. $\delta(.)$ is the *Dirac delta function*, describing a unit impulse.

Two types of TDL channels are used in simulations in this thesis: TDL-C-300 and TDL-C-1000, which are described in [51]. The number in the name of the channel model defines the *Root Mean Square* (RMS) delay spread of the signal in nano seconds. RMS delay spread is the standard deviation (i.e. root-mean-square) value of the delay of reflections, weighted proportional to the energy in the reflected waves. RMS delay spread is defined as:

$$\tau_{rms} = \sqrt{\frac{\int_0^\infty (\tau - \bar{\tau})^2 A_c(\tau) d\tau}{\int_0^\infty A_c(\tau) d\tau}}, \tag{5.2}$$

Where $A_c(\tau)$ is the power delay profile of the channel and $\bar{\tau}$ is the mean delay,

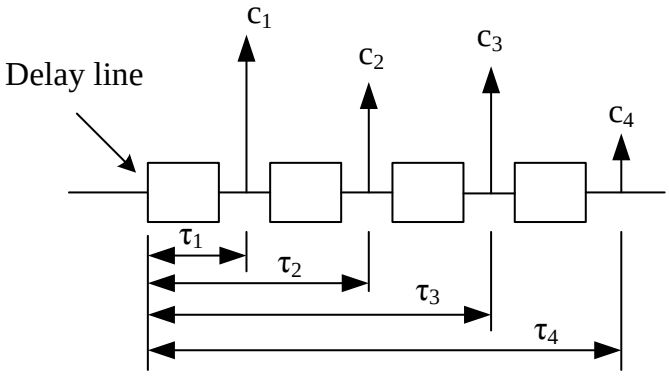

Figure 5.4 *Tapped delay line.*

which is is the average delay weighted by power (also known as the mean of access delay). Therefore, channel model parameters are scaled to correspond given 300 ns and 1000 ns RMS delay spread values for TDL-C-300 and TDL-C-1000 channel models, respectively.

5.4 Power Amplified Models

In this section, power amplifier models used in this thesis are presented. The non-linear characteristics of the *Power Amplifier* used to amplify the signal has to be considered, since it is the source of intermodulation products outside the channel bandwidth [15]. Different models are introduced for uplink and downlink, which are used in performance evaluations further in Chapters 6 and 7.

Generally, the key metric for quantifying the PA characteristics is backoff (BO). It measures the headroom between the average transmitted signal power and the maximum (saturated) output power of the PA. BO is defined as

$$BO = \frac{P_{max}}{P_{ave}}, \tag{5.3}$$

where P_{max} is the maximum output power of the PA and P_{ave} is the measured output level of PA. Backoff is usually denoted in dB scale. The required minimum backoff for sufficient transmitted signal quality is a waveform characteristic: waveforms with high PAPR are more sensitive to inevitable non-linearities of the PA [22].

In this thesis, input backoff (IBO) is used to measure the characteristics of used PA models. IBO is determined according to input referred 1-dB compression point ($P_{\text{1-dBp}}$), which is the input power value that causes the gain to decrease 1 dB from the normal linear gain specification. IBO value indicates the difference between the target input power level (P_{target}) and 1-dB compression point i.e. IBO = $P_{\text{1-dBp}}$ −

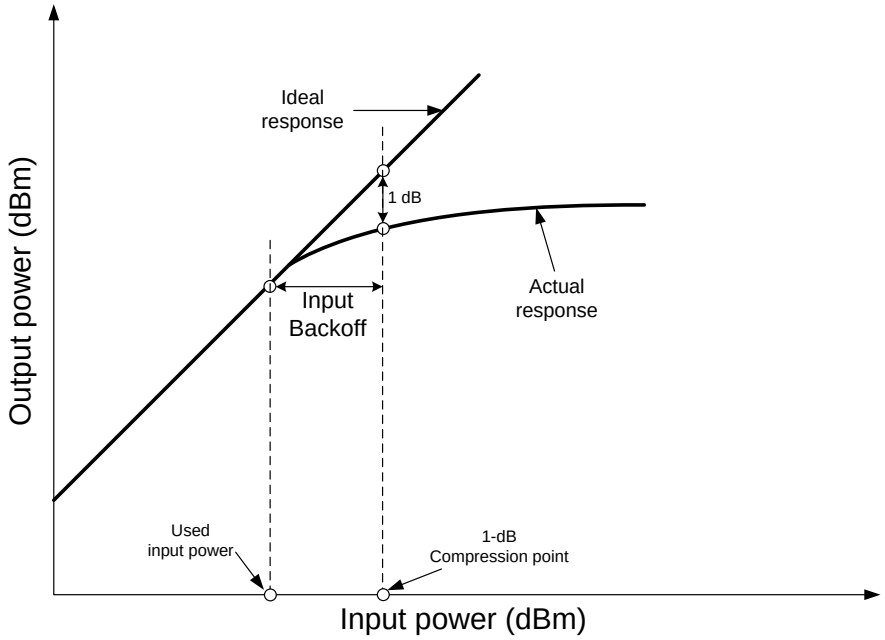

Figure 5.5 *Illustration of IBO determination.*

P_{target}. IBO determination is illustrated in Figure 5.5.

Effect of the power amplifier is examined in terms of spectral containment. In practise, the most harmful effect is increased out-of-band emission of the signal, which closes the spectrum gap between the transmitted signal and LTE spectrum mask. Effect of power amplifier is shown in Figure 5.6 (a), where *Power Spectral Density* (PSD) of W-OFDM signal is plotted before and after a power amplifier processing in green and red lines, respectively. 30 kHz measurement bandwidth is used to define DL LTE OBE mask plotted also in Figure 5.6 (a). Rapp PA model is used (determined in Section 5.4.1) and IBO value is se to 11.6 dB. It can be seen that well localized W-OFDM signal in PA input is effected strongly by a PA model, producing "shoulders" for the PSD. Basically the effect of PA model is not waveform related, and similar distortion takes places for each waveform in presence of transmitter PA.

Effect of the IBO value for LTE like CP-OFDM uplink fullband transmission with LTE OBE mask defined for 30 kHz measurement bandwidth is shown in Figure 5.6 (b). Used PA model is Polynomial model, which is considered in uplink transmission schemes (explained in more details in Section 5.4.2) and parametrization corresponds to a LTE parametrization for 10 MHz channel. It can be seen that the spectral leakage to adjacent channels is reduced when IBO value is higher, that is, the transmit power is lower. From Figure 5.5, it is notable that IBO can-

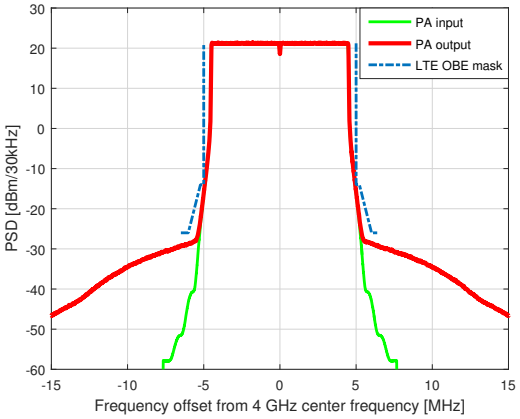

(a) W-OFDM signal before and after the Rapp PA modeling.

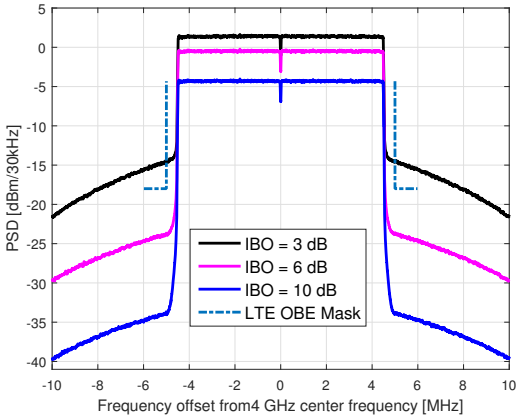

(b) Effect of IBO when using Polynomial PA model for LTE like CP-OFDM signal.

Figure 5.6 *PA effect in (a) DL Rapp model and effect of IBO in (b) UL Polynomial model.*

not be reduced arbitrarily, as the 3 dB IBO example exceeds the LTE OBE mask, whereas 6 dB and 10 dB IBO cases fits to the mask and can be used in such conditions. Thus, the trade-off between maximum PA output power and the out-of-band spectral leakage is considered depending on the system requirements.

5.4.1 Downlink PA model

The downlink PA model used in this thesis is a modified Rapp model which is introduced in [52]. This model mimics the base station PA including some crest factor reduction and digital predistortion schemes to linearise the base station PA. The Rapp model is defined as a combination of the amplitude-to-amplitude (AM-AM) distortion and amplitude-to-phase (AM-PM) distortion. AM-AM distortion is specified as

$$F_{AM-AM}(x) = \frac{G}{\left(1 + |\frac{Gx}{V_{SAT}}|^{2p}\right)^{1/(2p)}} \tag{5.4}$$

and AM-PM distortion as

$$F_{AM-PM}(x) = \frac{A|\frac{Gx}{V_{SAT}}|^{q}}{1 + |\frac{Gx}{BV_{SAT}}|^{q}} \tag{5.5}$$

where x is the instantaneous amplitude of the signal, gain G is normalized to $G = 1$, saturation voltage $V_{\mathrm{SAT}} = 239.6$ V at 50Ω load, smoothness factors are $P = 3$ and

$Q = 5$. A and B are set to $A = -0.14$ and $B = 1.2$. This model has $P_{\text{1-dBp}} = 57.6$ dBm (the input power is high because the gain in the model is set to unity). 11.6 dB input backoff is assumed in all uplink simulations, providing total output power $P_{\text{DL}} = 46$ dBm. The parametrization of PA is targeted to provide 46 dBm output power for 10 MHz fully populated LTE signal with 64-QAM, out-of-band adjacent channel leakage ratio of 45 dB and meeting the emission mask defined earlier in this section.

5.4.2 Uplink PA model

For uplink, the used PA model is a 9th order polynomial model, which is based on real measurements [53]. The polynomial coefficients are ordered from p_9 to p_0 defining the amplitude distortion as

$$\begin{aligned} p_{AM} = \; & [7.9726e-12, 1.2771e-9, 8.2526e-8, 2.6615e-6, 3.9727e-5, \\ & 2.7715e-5, -7.1100e-3, -7.9183e-2, 8.2921e-1, 27.3535], \end{aligned} \tag{5.6}$$

and phase distortion as

$$\begin{aligned} p_{PM} = \; & [9.8591e-11, 1.3544e-8, 7.2970e-7, 1.8757e-5, 1.9730e-4, \\ & -7.5352e-4, -3.6477e-2, -2.7752e-1, -1.6672e-2, 79.1553]. \end{aligned} \tag{5.7}$$

This polynomial model should be used only with input levels between -30 dBm and 9 dBm. Input related 1-dB compression point (illustrated in Figure 5.5) is at $P_{1-dBp} = 3.4$ dBm and the model is parametrized to provide 26 dBm output power for PA with 20 MHz bandwidth using fully populated *Quadrature Phase Shift Keying* (QPSK) modulated LTE uplink signal. In addition, ACLR requirement of 30 dB should be satisfied.

6. TRANSMITTER SIDE PERFORMANCE

In this chapter, evaluated waveforms are studied in terms of transmitter side performance. As discussed earlier in Section 5.4, PA has significant effect on transmitted signal spectrum. Thus, all cases are considered with a proper PA model, described in Section 5.4, to mimic real life conditions as well as possible. Evaluated performance metrics are first described and then the results of the enhanced CP-OFDM waveforms presented in this thesis are compared to LTE like reference waveforms.

The main focus of this chapter is to evaluate spectral localizations of considered waveforms, which describes the waveform characteristics in terms of power leakage to out-of-band frequencies. Power leakage to adjacent channels forces to use guard bands between different transmissions. Hence, the target is to reduce inband and out-of-band power leakage compared to the current LTE implementation and utilize the allocated spectrum more efficiently.

6.1 Evaluated Allocations

Transmitter side performance analysis is presented with two different allocation sizes. The LTE fullband allocation is a high throughput scenario utilizing the whole bandwidth whereas the narrowband transmission scheme models the data traffic of small burst. The future wireless communication systems should be flexible in order to serve rapidly changing service requirements, and thus, the transmitter performance for proposed waveforms are evaluated with these two allocation cases. All evaluations assume carrier frequency of 4 GHz.

6.1.1 Fullband Allocation

In LTE system, fullband allocation for 10 MHz channel bandwidth, consist of 50 PRBs as described in Chapter 5. 50 PRBs with LTE parametrization corresponds to a 9 MHz bandwidth (50 PRBs $\times$ 12 SCs $\times$ 15 kHz = 9000 kHz) in frequency domain, meaning that 1 MHz guard band is reserved for reducing power leakage to adjacent channel. The fullband case is considered as a high throughput scenario, which aims to maximize data rates of the transmission.

In order to improve maximum throughput, the fullband PRB allocation can be increased from 50 PRB in 5G NR. This is possible only if the LTE OBE spectrum mask (described in Section 5.2) is not exceeded. New waveforms introduced in this thesis targets to reduce OOB power leakage, which may allow to use more PRBs in fullband transmission inside the 10 MHz channel. This would improve the spectral efficiency, that is, the measure of how efficiently the spectrum can be used during data transmission. By increasing the spectral efficiency, the capacity of the network increases without the need to use more spectrum [3]. It is also emphasized in the current 3GPP TSG-RAN WG1 way forward [50], that 5G NR should support larger allocations in the same channel bandwidths as used in LTE, which is one likely scenario to increase spectral efficiency in 5G systems. LTE has bandwidth efficiency of 90% for a 10 MHz channel bandwidth (9 MHz/10 MHz $\times$ 100% = 90% efficiency), but it can be improved with better localized waveforms. Therefore, 52 PRB (93.6% efficiency) and 54 PRB (97.2% efficiency) allocations are also examined here in terms of PSD fitting to the LTE OBE mask.

6.1.2 Narrowband 1 PRB Allocation

Another examined allocation size is 1 PRB allocation. It can be considered as a important case from two perspectives. Firstly, it can be considered as the minimum allocation for a UE on a cell edge trying to keep the connection alive in coverage limited scenarios, where throughput is not that significant. Secondly, it can be considered as a low data-rate connection from a different service category which is transmitting narrowband signal inside the fullband enhanced mobile broadband (eMBB) channel.

Mixed numerology transmission schemes inside a LTE eMBB channel is a potential scheme for 5G networks e.g. for Internet of Things (IoT) or machine-to-machine (M2M) type services. What is interesting in the scope of this thesis, is that the packet sizes can vary rapidly as the traffic is predicted to contain more small burst communications. That is due to the increasing usage of sensor devices (e.g. temperature sensors) and smartphone functionalities (e.g. incremental updates for stock exchange apps) sporadically transmitting very small packets [37]. Hence, the narrowband transmission scheme is relevant case when 5G NR is researched.

6.2 Spectral Localization

One of the most important feature for waveforms used in advanced wireless communications is the so called *spectral localization*, which describes how well a transmission

fits into the allocated bandwidth while trying to minimize the out-of-band power leakage. When the spectral localization is improved, less guard bands are needed to ensure a desirable signal quality. This allows to use wider band for transmission which increases spectrum efficiency.

In this section, PSDs of FC-F-OFDM and W-OFDM waveforms are compared against CP-OFDM waveform to evaluate improvement of spectral localization. The PSD is evaluated per subframe and 100 independent realization at the PA output are averaged in the results. 30 kHz measurement bandwidth is assumed to define the LTE OBE mask in DL and UL, which are presented in Section 5.2.

6.2.1 Fullband PSD

When examining spectral localization in fullband case, PSD is plotted after power amplifier modeling in transmitter processing chain and MCS 64-QAM, $R = 3/4$ is used. For 64-QAM, the EVM requirement is 8% [49] and here it is assumed that PA may contribute 5%, and rest of the distortion is caused by other sources as phase noise, I/Q imbalance, etc. Input backoff values for UL fullband cases are searched with 0.1 dB steps, which is done for each waveform and allocation size individually, while fulfilling LTE OBE mask for UL and 5% EVM requirement. For downlink, the IBO is not adjustable as it is set to constant value 11.6 dB (the Tx power is fixed to 46 dBm as explained in Section 5.4).

At first, fullband transmission scheme is considered using 50 PRB allocation corresponding to the current LTE fullband allocation. Figure 6.1 (a) shows the 50 PRB allocation size PSD for uplink with minimum achieved IBO values listed in Table 6.1. As the EVM requirement is the limiting factor and restricts the Tx power[1] from PA output, IBO values are rather high in UL 50 PRB allocation. Thus, all waveforms fit into the LTE OBE mask clearly and the difference between waveforms are not significant in uplink case. The low UL Tx power is due to highly non-linear UE PA model which indicates that in the UL, the differences between waveform signal processing are reduced, especially in fullband case. Only the DFTs-OFDM waveform differs slightly from other as it has better PAPR characteristics allowing to use higher transmission powers.

In DL transmission scheme, which has stricter OBE restrictions, the gap between LTE OBE and PSDs is much smaller than in UL as seen Figure 6.1 (b). FC-F-OFDM and CP-OFDM fits to the mask by eye, but the PSD of the W-OFDM signal comes

[1]Here, PA output power is denoted as Tx power. Typically e.g. 4 dB of losses is assumed after PA when defining transmitted power of the whole transmitter chain output.

Table 6.1 *Maximum Tx power with corresponding IBO and EVM for UL fullband allocation of 50 PRB.*

	IBO [dB]	Tx Power [dBm]	EVM
CP-OFDM	12.6	17.64	5.0
W-OFDM	12.6	17.64	4.9
FC-F-OFDM	12.6	17.64	5.0
DFTs-OFDM	11.0	19.32	5.0

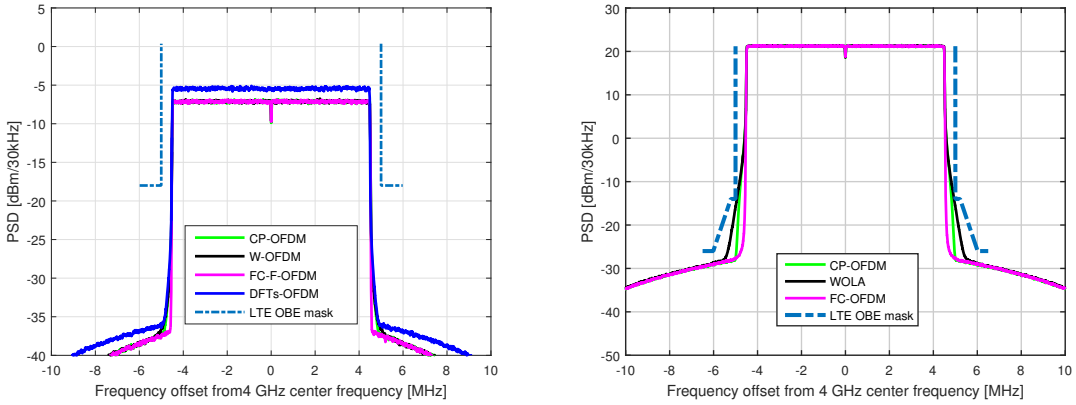

(a) 50 PRB fullband PSDs in UL.

(b) 50 PRB fullband PSDs in DL.

Figure 6.1 *Fullband PSD of 50 PRB allocation in (a) UL and (b) DL for FC-F-OFDM, W-OFDM and CP-OFDM. For UL, DFTs-OFDM is evaluated as well.*

closer to the LTE OBE mask. In Figure 6.2, the critical area is zoomed to see more accurately the behaviour of the DL fullband PSDs. It can be seen that W-OFDM stays under the LTE mask, whereas FC-F-OFDM performs better in terms of spectral localization. It should be noted that W-OFDM has worse fullband spectral localization than CP-OFDM and does not bring any gain in that manner. The extra band between waveform envelope and LTE mask for W-OFDM and FC-F-OFDM are 66 kHz and 435 kHz, respectively. Therefore, especially a FC-F-OFDM signal, has a potential for even higher PRB allocations than 50. That is an interesting feature as 5G NR targets for higher data rates by supporting larger allocations in the same channel bandwidths as used in current LTE system.

As the results in Figure 6.1 show, the allocation of more than 50 PRBs might fit also in to the LTE OBE mask inside a 10 MHz LTE channel, especially in case of FC-F-OFDM. Here, the fullband allocation is extended to 52 PRB and 54 PRB and corresponding PSDs are shown in Figures 6.3 and 6.4 to observe a potential of waveforms for extended fullband allocation sizes. MCS 64-QAM, $R = 3/4$ is used

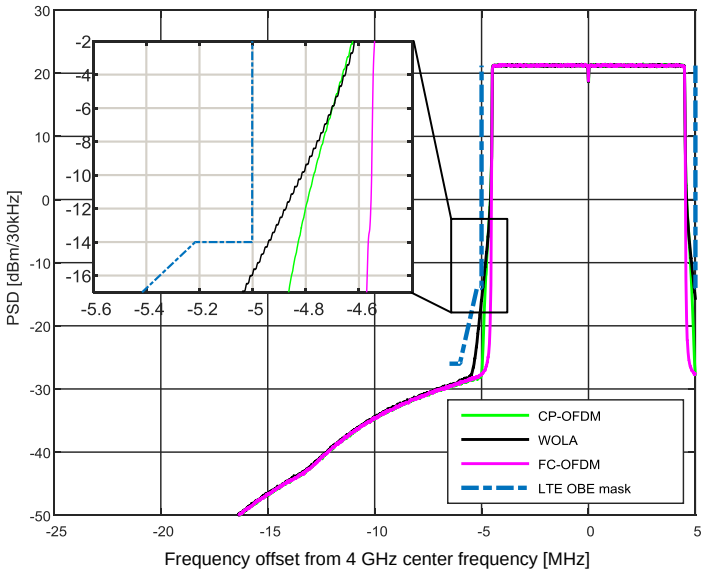

Figure 6.2 *Downlink 50 PRB PSDs, zoomed close to LTE OBE mask.*

determining EVM requirement of 5% and IBO values for UL cases are searched for each allocation sizes individually. IBO values for 52 PRB and 54 PRB allocations are listed in 6.2 and 6.3, respectively. PSD figures are zoomed to the left side of the channel for more accurate observations of LTE OBE mask violations. It is enough to consider only one side of the spectrum as waveforms are symmetrical around the used center frequency (4 GHz).

Table 6.2 *Maximum Tx power with corresponding IBO and EVM for UL fullband allocation of 52 PRB.*

	IBO [dB]	Tx Power [dBm]	EVM
CP-OFDM	12.6	17.64	5.0
W-OFDM	12.6	17.64	5.0
FC-F-OFDM	12.6	17.64	5.0
DFTs-OFDM	11.0	19.32	5.0

Figures 6.3 (b) and 6.4 (b) shows that all waveforms satisfies the LTE OBE mask in UL extended fullband cases and the differences between the waveforms are not significant as already observed in 50 PRB case. 5% EVM requirement is here the limiting factor as well and waveforms fits to the LTE OBE mask due to the low transmission powers. DFTs-OFDM has again slightly better characteristics to overcome PA non-linearities contributing lower EVM values, and thus, the maximum Tx power is highest.

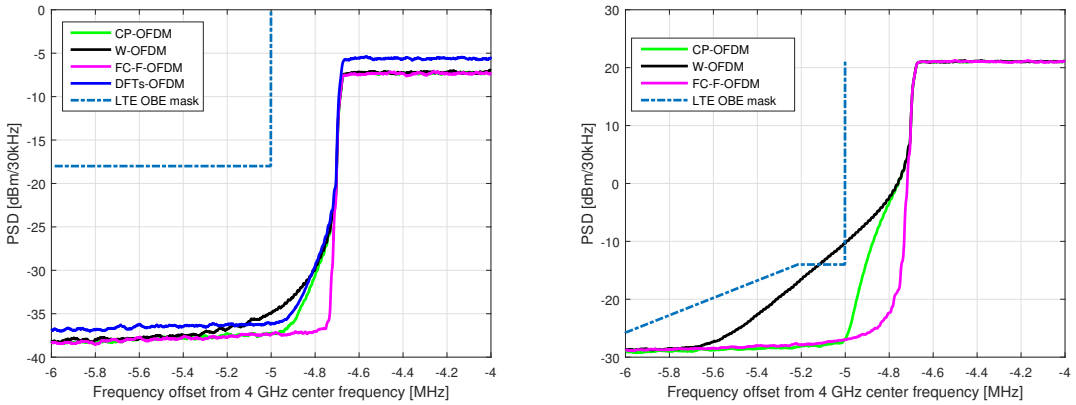

(a) Fullband PSDs in uplink using 52 PRBs. (b) Fullband PSDs in downlink using 52 PRBs.

Figure 6.3 *52 PRB Fullband PSD illustration of FC-F-OFDM, W-OFDM and CP-OFDM in (a) UL and (b) DL. For UL, DFTs-OFDM is evaluated as well.*

In DL, more strict LTE OBE mask becomes problematic in the extended fullband PSD evaluations. It was noticed in 50 DL PSD evaluations, that W-OFDM has worse spectral localization than CP-OFDM and FC-F-OFDM, and thus, it does not fit inside the LTE OBE mask in cases having higher allocation than 50 PRB (see Figures 6.3 (a) and 6.4 (a)). That was an expected result as the W-OFDM had small extra band between spectrum and LTE OBE mask and it almost exceeded the mask already with 50 PRB allocation (see Figure 6.2). The IBO values are not adjustable in DL, and thus, additional techniques such as channel filtering for W-OFDM would be needed to overcome LTE OBE mask in these 5G NR relevant extended fullband allocations. However, FC-F-OFDM spectra in both 52 PRB and 54 PRB allocations fit well to the LTE OBE mask in DL while CP-OFDM stays slightly under the LTE OBE mask in both cases. In addition, FC-F-OFDM achieves 54 kHz more band between LTE OBE mask than CP-OFDM. Thus, FC-F-OFDM can be considered as a better option than W-OFDM in terms of spectral efficiency for high throughput scenarios.

Table 6.3 *Maximum Tx power with corresponding IBO and EVM for UL fullband allocation of 54 PRB.*

	IBO [dB]	Tx Power [dBm]	EVM
CP-OFDM	12.6	17.64	5.0
W-OFDM	12.5	17.75	5.0
FC-F-OFDM	12.6	17.64	5.0
DFTs-OFDM	11.0	19.32	5.0

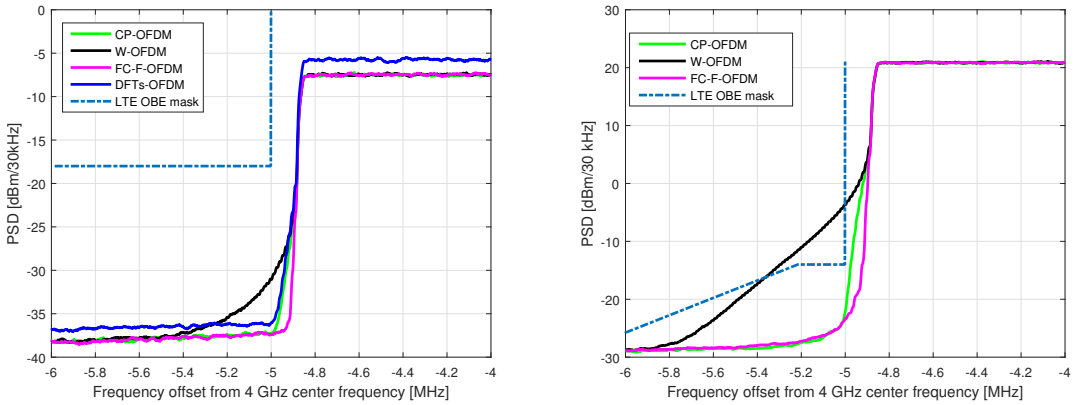

(a) Fullband PSDs in uplink using 54 PRBs. (b) Fullband PSDs in downlink using 54 PRBs.

Figure 6.4 *54 PRB Fullband PSD illustration of FC-F-OFDM, W-OFDM and CP-OFDM in (a) UL and (b) DL. For UL, DFTs-OFDM is evaluated as well.*

6.2.2 Narrowband PSDs and maximum transmit power

In 1 PRB allocation transmission scheme, the active PRB is located at the left edge of the channel, being the first set of subcarriers inside the fullband allocation. This models the UL 1 PRB transmission scheme, where mobile terminal is transmitting a narrowband low rate signal, and thus, the polynomial PA model is used for narrowband PSD results. PSD of the waveforms with 1 PRB allocation is shown in Figure 6.5 (a) for 50 PRB maximum allocation and in Figure 6.5 (b) for 54 PRB maximum allocation. The only difference is that the allocation size is located closer to the LTE OBE mask in 54 PRB maximum allocation as it occupies wider frequency band.

For 1 PRB narrowband allocation, the maximum PA output power is the most interesting metric. MCS is reduced to QPSK, $R = 1/2$ which is more robust against interferences, but does not provide as high maximum throughput (than 64-QAM or 256-QAM) as the target is to maximize receiver side (Rx) power spectral density in the Base Station (BS) side rather than throughput. EVM requirement of 17.5% for QPSK was obtained from [49] and it is assumed here that PA may contribute 12%, and rest of the distortion is caused by other sources. The observed maximum Tx powers, corresponding IBO values and EVM values for each waveform in 1 PRB case with 50 PRB and 54 PRB maximum allocation are shown in Tables 6.4 and 6.5, respectively.

In case of 50 PRB maximum allocation, EVM requirement of 12% is the limiting factor. The distance between the first PRB and LTE OBE mask is large enough that violating the mask is not a problem for any waveform spectrum (see Figure 6.5)

(a). Hence, all waveforms stays clearly under the LTE OBE mask and Tx output powers are similar. DFTs-OFDM has the best PAPR characteristics which results in lower EVM values after the PA processing allowing to use higher transmitter powers. FC-F-OFDM has the best spectral localization producing rather low power leakage to both sides of the allocation. W-OFDM waveform is closest to LTE OBE mask but it suppress the power leakage symmetrically on both sides as well, which is a desirable feature. Channel filter used in CP-OFDM and DFTs-OFDM filters the left hand side of the signal as it is the channel edge, but the power leakage to the right hand side is not suppressed. This leads to a high interference powers in adjacent inband channels.

Table 6.4 *UL 1 PRB max Tx Power and EVM when maximum allocation size is 50 PRB.*

	IBO [dB]	Tx Power [dBm]	EVM
CP-OFDM	4.6	25.37	12.0
W-OFDM	4.6	25.40	11.7
FC-F-OFDM	4.7	25.30	11.8
DFTs-OFDM	2.2	27.55	11.5

Table 6.5 *1 PRB max Tx Power and EVM when maximum allocation size is 54 PRB.*

	IBO [dB]	Tx Power [dBm]	EVM
CP-OFDM	7.3	23.21	6.9
W-OFDM	14.8	15.25	2.9
FC-F-OFDM	7.5	23.01	7.4
DFTs-OFDM	6.3	24.37	7.7

When the maximum allocation size for 10 MHz channel is increased to 54 PRBs, the LTE OBE mask becomes the limiting factor as the active PRB is located closer to the channel edge. Channel filters used in CP-OFDM and DFTs-OFDM waveforms are specified precisely for 54 PRB allocation size. From figure 6.5 (b), it can be seen that the W-OFDM has lower Tx power than other waveforms. This is due to the higher power leakage, which restricts the Tx power critically in W-OFDM case, as the OBE LTE mask is the limiting factor. Other waveforms have similar maximum Tx powers as the channel filter attenuates CP-OFDM and DFTs-OFDM signals in the channel edge. Difference between CP-OFDM and DFTs-OFDM is now reduced as the LTE OBE mask is the limiting factor. However, it should be noted that FC-F-OFDM has again significantly lower power leakage to right hand side of the allocation than CP-OFDM and DFTs-OFDM. As the W-OFDM has also a same

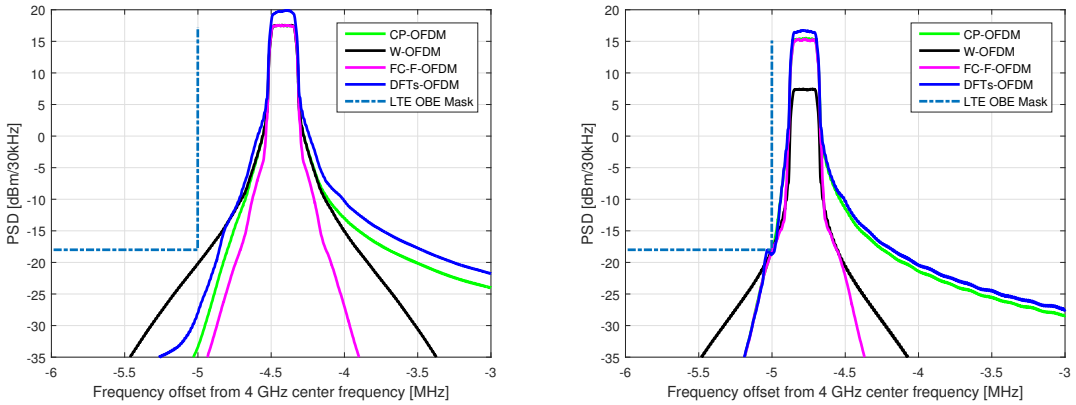

(a) Maximum allocation 50 PRB. (b) Maximum allocation 54 PRB.

Figure 6.5 *PSDs of 1 PRB allocation and LTE OEB uplink mask in the cases of maximum allocation sizes of (a) 50 PRB and (b) 54 PRB.*

symmetrical suppression feature, it may be useful when using additional filtering methods.

In addition, maximum Tx power for 4 PRB allocation with MCS of 64-QAM, $R = 3/4$ is researched here, which is used in most simulations in Chapter 7 to model low data-rate service inside the 10 MHz LTE channel. Therefore, the uplink PSDs with 4 PRB allocation are illustrated in Figure 6.6. EVM requirement for 64-QAM is 8% [49] and here it is assumed that PA may contribute 5%.

Table 6.6 *UL 4 PRB max Tx Power and EVM when maximum allocation size is 50 PRB.*

	IBO [dB]	Tx Power [dBm]	EVM
CP-OFDM	12.5	17.75	5.0
W-OFDM	12.5	17.75	5.0
FC-F-OFDM	12.8	17.4	5.0
DFTs-OFDM	11.0	19.32	4.9

Similar to 1 PRB case, the limiting factor is the tight EVM requirement for 64-QAM for 50 PRB maximum allocation, whereas the LTE OBE mask is not an issue here. These IBO values, which corresponds to the maximum Tx powers, are used for each waveform individually in UL simulations in Chapter 7. Similar observations can be made here than in 1 PRB case: FC-F-OFDM has clearly lower power leakage than W-OFDM and both waveform candidates suppress the inband power leakage significantly better than CP-OFDM or DFTs-OFDM.

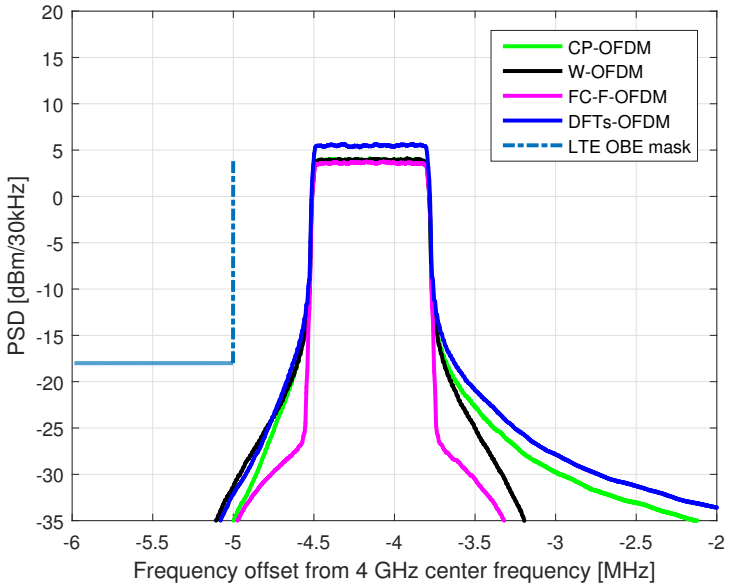

Figure 6.6 *PSDs of 4 PRB allocation and LTE OBE uplink mask in the cases of maximum allocation sizes 50 PRB.*

6.3 Adjacent Channel Leakage Ratio

In practise, all functional waveforms used in wireless communications produces unwanted emissions consisting of OOB emissions and spurious emissions [54]. In addition to OBE masks, the out-of-band emissions requirement for the transmitter is generally specified in terms of *Adjacent Channel Leakage Ratio* (ACLR). It is the ratio of the average power between assigned channel and average leakage power to adjacent channel, usually expressed in dB. ACLR is defined as:

$$10log_{10} \times \left(\frac{mean(P_{assigned})}{mean(P_{adjacent})} \right) dB, \tag{6.1}$$

where P_{assigned} is the average power of all assigned subcarriers in the desired channel and P_{adjacent} is the average leakage power in the subcarriers of the adjacent channel. Function mean$(\cdot)$ calculates simply the average value of all vector elements, that is, powers of subcarriers in this case. For current LTE system, ACLR requirements for LTE uplink and downlink are defined in [49] and [48] respectively.

6.3.1 Fullband ACLR

In fullband scheme (50 PRB allocation), which corresponds to a 9 MHz transmission bandwidth, the adjacent channel is determined as the neighboring frequency

band equal size to the transmission bandwidth, called as Out-of-Band ACLR (OOB ACLR). Here two different OOB ACLR cases are considered. In the first case, the adjacent channel is determined to begin immediately after the active band i.e. there is no inactive subcarriers between evaluated bands. This is illustrated in Figure 6.7 (a), where powers of *Active band* and *Adjacent channel* are denoted as P_{assigned} and P_{adjacent}, respectively. The IBO value in fullband ACLR evaluations is set to 4.8 dB, when all waveforms stays slightly under the LTE OBE mask in 50 PRB fullband case (EVM requirement is ignored as the purpose is to study power leakage).

Second OOB ACLR case is more practical, modeling LTE 10 MHz transmission scheme and power leakage to adjacent 10 MHz channel. As the transmission bandwidth equals to 9 MHz, there is 500 kHz unallocated band at the both edges of the 10 MHz channel, which is generally called as *Guard Band* (GB). In this scheme, two neighboring 10 MHz channels are transmitting fullband signal, and thus, the GB between active bands is $2 \times 500\ kHz = 1000\ kHz = 1\ MHz$ wide, illustrated in Figure 6.7 (b). P_{assigned} and P_{adjacent} are determined similarly to the first OOB ACLR case and IBO value is 4.8 dB.

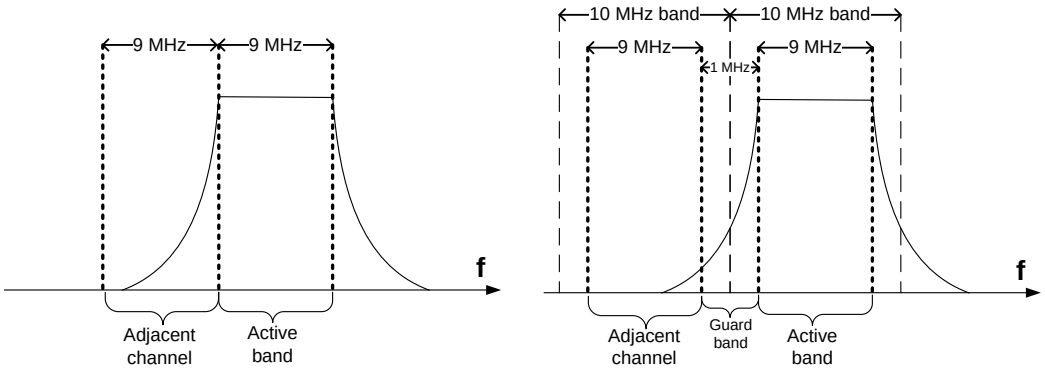

(a) OOB ACLR without GB.

(b) OOB ACLR in 10 MHz LTE channel.

Figure 6.7 *Illustration of Out-of-Band ACLR calculations with 50 PRB fullband allocation (a) without and (b) with guard band.*

The OOB ACLR results for proposed 5G NR waveforms FC-F-OFDM and W-OFDM are compared to reference waveforms and are shown in Table 6.7. All waveforms have similar OOB ACLR performance without significant observations. Channel filtering used in CP-OFDM is precisely designed for fullband transmission having proper OOB ACLR performance in fullband ACLR evaluations. Considerable observation here is that W-OFDM and FC-F-OFDM do not fall behind from CP-OFDM OOB ACLR values at all.

In uplink, none of the waveforms achieves E-UTRA ACLR target for uplink, which

Table 6.7 *Out-of-Band ACLRs in DL and UL transmission scheme with GB = 0 and 1 MHz.*

ACLR [dB]	UL, GB= 0	UL, GB= 1 MHz	DL, GB= 0	DL, GB= 1 MHz
CP-OFDM	20.2	25.1	22.7	54.4
W-OFDM	20.2	25.0	22.6	54.4
FC-F-OFDM	20.3	25.1	22.9	54.4
DFTs-OFDM	22.9	28.8	-	-

is 30 dB [49]. Next, minimum IBO values to achieve 30 dB ACLR are studied for GB = 1 MHz and the results are listed in Table 6.8. ACLR UL requirement cannot be achieved without a GB, and thus, GB = 0 is not studied here. As expected according to results in Table 6.7, CP-OFDM, FC-F-OFDM and W-OFDM have rather similar minimum IBO values, which are increased around 2 dB to achieve 5 dB increase in ACLR values approximately. DFTs-OFDM allows to use higher Tx power here as well and the IBO is increased by 0.4 dB in order to have 1.3 dB improvement in ACLR.

Table 6.8 *Minimum IBO for waveforms to achieve 30 dB uplink ACLR requirement with GB = 1 MHz.*

ACLR [dB]	ACLR [dB]	IBO [dB]
CP-OFDM	30.0	6.8
W-OFDM	30.0	6.8
FC-F-OFDM	30.3	6.9
DFTs-OFDM	30.1	5.2

Table 6.9 *GB required for each waveform to satisfy 45 dB downlink ACLR requirement.*

ACLR [dB]	ACLR [dB]	GB [kHz]
CP-OFDM	45.0	194
W-OFDM	45.0	242
FC-F-OFDM	45.3	63

E-UTRA ACLR target for DL is 45 dB [48], which is achieved by each waveform with GB of 1 MHz, whereas ACLR requirement cannot be achieved without a GB. As the IBO is not adjustable in DL Rapp model, guard band required to achieve 45 dB ACLR is researched and results are shown in Table 6.9. W-OFDM requires the largest GB (242 kHz) due to the slowest power leakage suppression as seen in Figure 6.2. FC-F-OFDM needs only 64 kHz to achieve 45 dB ACLR, which is improved

by 22.4 dB. Hence, 131 kHz less guard band is needed for FC-F-OFDM than CP-OFDM whereas W-OFDM requires 48 kHz larger GB than CP-OFDM, which can be seen in spectral containment of the waveforms in Figure 6.2.

6.3.2 1 PRB narrowband ACLR

Transmission scheme of 1 PRB allocation has gained more interest in 5G development as discussed earlier in Section 6.2.2. Therefore, *Inband ACLR* is an interesting metric when examining features of the narrowband transmission. It models the inband transmission scheme, where multiple narrowband uplink signals are transmitted inside the one wideband channel (e.g. 10 MHz LTE channel). These narrowband signals can originate from several different services or devices operating with different parametrization. Hence, the power leakage of the narrowband transmission becomes a crucial factor to minimize GB between signals. Lower power leakage improves the spectral efficiency and more narrowband transmissions are allowed inside one channel.

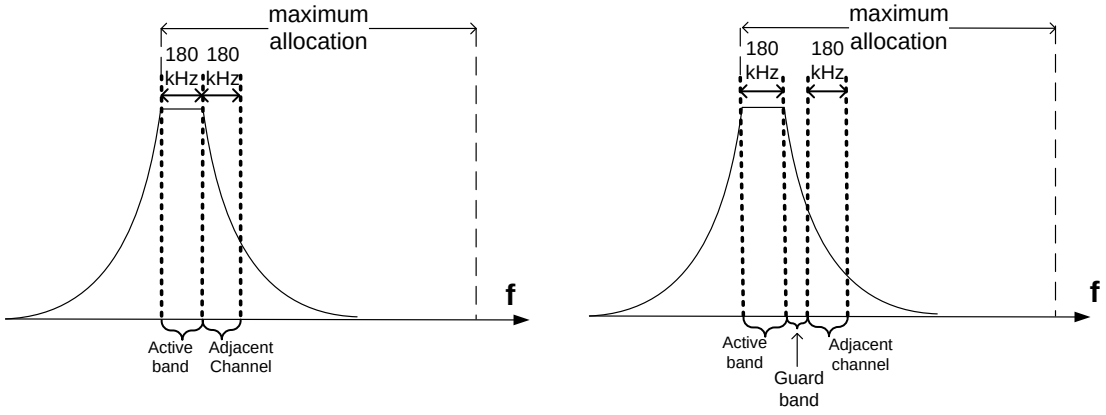

(a) Inband ACLR without guard band.

(b) Inband ACLR with with guard band.

Figure 6.8 *Illustration of inband ACLR calculation (a) wihtout and (b) with guard band.*

In inband ACLR calculations, active narrowband signal is located to left channel edge as discussed earlier in this chapter. Thus, the adjacent channel used in inband ACLR calculations is the next band inside the channel i.e. it is located on the right hand side of the active band, which is demonstrated in Figure 6.8 (a). This models a UL scenario with possibly multiple narrowband transmission inside the channel bandwidth, and thus, the polynomial PA model is used in inband ACLR evaluations. In Section 6.2.2, the MCS was chosen to be QPSK, $r = 1/2$ for 1 PRB allocations. Waveform specific IBO values, which are listed in Table 6.4, are set for

each waveform individually corresponding to maximum Tx power evaluations in 50 PRB maximum allocation case.

Similar to fullband case, in most cases the GB is needed between narrowband signals to deal with the power leakage. The guard band is expressed as a number of PRBs (1 PRB = 12 SCs $*$ 15 kHz = 180 kHz) to be disabled between signals, which can be implemented easily with proper scheduling. Guard bands of 0, 180, 360 and 540 kHz are considered corresponding 0,1,2 and 3 disabled PRBs between narroband signals. The usage of a guard band in inband ACLR calculations is demonstrated in 6.8 (b).

Table 6.10 *Inband ACLR of 1st, 2nd, 3rd, 4th neighboring PRBs in 1 PRB uplink case.*

ACLR [dB]	GB=0 kHz	GB=180 kHz	GB=360 kHz	GB=540 kHz	IBO [dB]
CP-OFDM	16.9	28.4	32.5	35.1	4.6
W-OFDM	17.1	29.8	35.9	41.2	4.6
FC-F-OFDM	18.2	38.6	51.9	58.9	4.7
DFTs-OFDM	16.7	28.2	32.2	34.9	2.2

The inband ACLR results, which are based on PSDs plotted in 6.5 (a), are shown in Table 6.10. It can be seen that FC-F-OFDM has a superior performance compared to DFTs-OFDM, CP-OFDM and W-OFDM. FC-F-OFDM is the only candidate achieving inband ACLR above 30 dB with 1 PRB GB, and provides more than 1 dB gain compared to other waveforms in the 0 GB case, which results from superb narrowband filtering properties of FC-F-OFDM. W-OFDM improves inband ACLR performance compared to CP-OFDM due to the symmetric power leakage attenuation feature. Nevertheless, time domain windowing does not suppress side lobes as well as FC based filtering, meaning that wider guard band does not gain similar improvement in inband ACLR values than in FC-F-OFDM case. That results lower inband ACLR values especially with widest GB (540 kHz), where the difference between W-OFDM and FC-F-OFDM is 17.7 dB.

Poor inband ACLR performance of CP-OFDM is originates from the channel filtering feature, which filters signal only at the channel edges. Narrowband signal is located in the left edge of the channel, meaning that right side of the signal is not filtered at all (illustrated in Figure 6.5 (a)). That leads to a high leakage to neighboring narrowband channels, and thus, for low inband ACLR values. In case of 540 kHz guard band, CP-OFDM have 6.1 dB and 23.8 dB lower inband ACLR values than W-OFDM and FC-F-OFDM, respectively. The same problem can be

noticed in case of DFTs-OFDM, which includes channel filtering as well. ACLR values are low, but it should be noted that max Tx power of the DFTs-OFDM is superior compared to other waveforms (see Table 6.4). That high maximum Tx power is a useful feature in 1 PRB case for example in coverage limited scenario.

6.4 Complexity comparison of evaluated waveforms

In this section, complexity of the W-OFDM and FC-F-OFDM is studied. In addition to overall performance, computational complexity is an important metric of waveform processing especially in UE side, where the device is size and power restricted. The complexity is measured by the number of real multiplications needed per CP-OFDM symbol in transmitter processing. Both waveform processing methods to be evaluated (W-OFDM and FC-F-OFDM) are implemented on top of CP-OFDM, which is based on FFT/IFFT pair, and their complexity is examined first. This is used as a baseline result for waveform specific complexity evaluations.

6.4.1 FC-F-OFDM complexity evaluations

When studying FC-F-OFDM computational complexity, the FFT/IFFT operation complexity is examined first, as it is the core module in both types of filter banks. For given transform length, FFT and IFFT have the same complexity, so only FFT complexity is considered here. For FFT complexity, the split-radix algorithm is commonly considered to be the most efficient one [55], if the transform length is a power of two. Applying split-radix algorithm, the number of real multiplications in FFT processing is

$$\mu_N = N(\log_2(N) - 3) + 4, \tag{6.2}$$

where N is a power of two transform length [55]. The number of real multiplication for the low rate transform used in FC-processing is expressed as

$$C_{\mathrm{OFDM}} = \sum_{m=1}^{M} N_{\mathrm{SYM}} \mu_{L_{\mathrm{OFDM},m}}, \tag{6.3}$$

where M is the number of subbands and $\mu_{L_{\mathrm{OFDM},m}}$ is the number of real multiplications required for IFFT of size $L_{\mathrm{OFDM},m}$ and N_{SYM} is the number of OFDM symbols. Here, the fullband allocation is assumed and we evaluate the complexity per one symbol over one subband (50 PRBs), meaning that $N_{\mathrm{SYM}} = 1$ and $M = 1$. Consequently, the number of real multiplication per symbol can be expressed as

$$M_{\mathrm{TOT,OFDM}} = C_{\mathrm{OFDM}}/N_{\mathrm{ACT},m}, \tag{6.4}$$

where N_{ACT} is the number of active subcarriers.

In fullband FC-F-OFDM, FFT size of $L_{\mathrm{OFDM},m} = 1024$ is used. Hence, the number of real multiplications for the OFDM transmitter processing for one OFDM symbol becomes $C_{\mathrm{OFDM}} = 1024 \times (log_2(1024) - 3) + 4 = 7172$ applying the Equation (6.2).

The number of blocks needed for the FC Tx processing is determined by

$$T_{\text{FC-BLOCKS},m} = \left\lceil \frac{(L_{\mathrm{OFDM},m} + L_{\mathrm{CP},m})N_{\mathrm{SYM}} + L_{\mathrm{O},m} - L}{L_{\mathrm{S},m}} \right\rceil + 1, \tag{6.5}$$

where $L_{\mathrm{OFDM},m}$ and $L_{\mathrm{CP},m}$ are the OFDM IFFT and CP lengths, respectively, on subband m. L_m is the forward transform size for subband m, $L_{\mathrm{O},m} = \lambda L_m$ is the number of overlapping samples in FC processing on subband m with the overlapping factor of λ, $L_{\mathrm{S},m} = L_m - L_{\mathrm{O},m}$ is the corresponding number of non-overlapping samples.

The number of real multiplications required for the FC processing becomes

$$C_{\mathrm{FC}} = T_{\text{FC-BLOCKS}} \left(\mu_N + \sum_{m=1}^{M} \left[\mu_{L_m} + 2\xi k_{\mathrm{TB}} \right] \right), \tag{6.6}$$

where μ_{L_m} and μ_N are the number of multiplications needed for the forward and inverse transforms of length L_m and N, respectively, and k_{TB} is the number of transition-band weights. For real-valued weights $\xi = 2$, which is used here.

Finally, the number of multiplications per symbol can be expressed as

$$M_{\mathrm{TOT,FC}} = \frac{C_{\mathrm{OFDM}} + C_{\mathrm{FC}}}{N_{\mathrm{SYM}} \sum_{m=1}^{M} N_{\mathrm{ACT},m}}, \tag{6.7}$$

where $N_{\mathrm{ACT},m}$ is the number of active subcarriers on subband m.

Complexity evaluations are performed over one subband ($m = 1$), which is in this case 50 PRB. LTE parameters listed in Table 5.1 are used here i.e. $N_{\mathrm{ACT},m} = 600$, $L_{\mathrm{OFDM},m} = 1024$ and $L_{\mathrm{CP},m} = 72$. Even though the complexity is evaluated per one symbol, the number of symbols is set to $N_{\mathrm{SYM}} = 1000$ for FC-F-OFDM evaluations in order to model continuous transmission. This has a significant effect to the complexity results due to the overlapping processing of FC-F-OFDM. In Section 5.2.3, transition bandwidth and overlapping factor are set to $k_{\mathrm{TB}} = 3$ and $\lambda = 1/2$. Transform lengths (L_m and N) are 1024, and thus, $\mu_{L_m} = \mu_N = 7172$ real

multiplications are required with split-radix algorithm, as calculated earlier in this section.

Using aforementioned parameters, the total number of real multiplications in FC-F-OFDM transmitter processing becomes $M_{\mathrm{TOT,FC}} \approx 63.2$ per symbol. For conventional OFDM, the corresponding result is $M_{\mathrm{TOT,OFDM}} = 7172/600 \approx 11.9$, meaning that for each symbol the FC-F-OFDM processing has around five times higher complexity.

6.4.2 W-OFDM complexity evaluations

In W-OFDM transmitter processing, the number of multiplications is simple to evaluate. Windowing is done in time domain, which means that window size N_{ws} (in samples) equals the number of additional complex multiplications needed for one symbol. Windowing is performed in both edges of the symbol meaning that $N_{ws}/2$ samples are windowed in both edges of the symbol. Each windowed sample is multiplied with the corresponding window value as illustrated in Figure 6.9. For simpler illustration, the window length of $N_{ws} = 10$ is chosen and only the right side of the windowed symbol is presented as the windowing is symmetrical in both symbol edges.

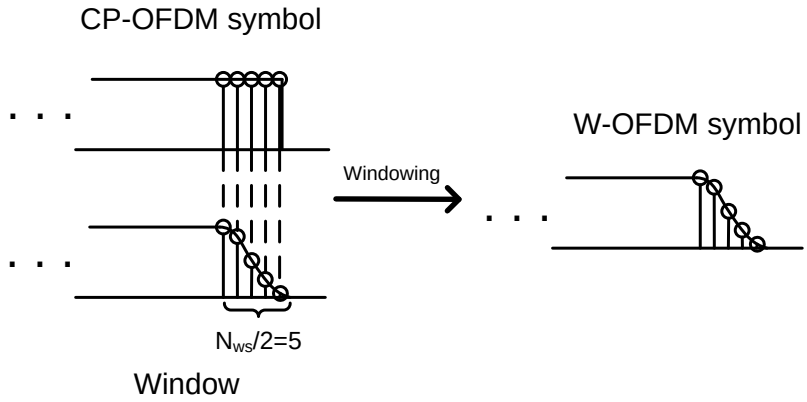

Figure 6.9 *W-OFDM sample wise complex multiplications in windowing processing.*

In order to evaluate the number real multiplications, the number of complex multiplication is doubled, as the real and imaginary parts of the symbol is windowed separately. Hence, the total number of multiplications in W-OFDM transmitter processing becomes

$$M_{\mathrm{TOT,W}} = \frac{C_{\mathrm{OFDM}} + 2C_{\mathrm{W}}}{N_{\mathrm{SYM}} \sum_{m=1}^{M} N_{\mathrm{ACT},m}}, \tag{6.8}$$

where C_{W} is the number of complex multiplications originated from the windowing operation.

In W-OFDM case, only one symbol i.e. $N_{\mathrm{SYM}} = 1$ as the complexity is not proportional to number of symbols. Similar to the FC-F-OFDM, the W-OFDM complexity is evaluated over 1 PRB ($M = 1$ and $N_{\mathrm{ACT},m} = 600$) and the $C_{\mathrm{OFDM}} = 7172$. The window size used in this thesis is chosen to $N_{ws} = 36$ (see Section 5.2.2), and thus, the number of additional complex multiplications is $C_{\mathrm{W}} = 36$. Finally, the total number of real multiplications becomes $M_{\mathrm{TOT,W}} \approx 12.1$. The number of real multiplication of W-OFDM transmitter processing is compared against conventional OFDM and FC-F-OFDM (studied in Section 6.4.1) in Table 6.11.

Table 6.11 *Complexity comparison of enhanced OFDM techniques against plain CP-OFDM without channel filtering.*

Plain CP-OFDM	W-OFDM	FC-F-OFDM
11.9	12.1	63.2

Significant difference between enhanced OFDM waveforms can be seen in terms of complexity. The W-OFDM transmitter processing does not increase the complexity significantly, whereas the FC-F-OFDM transmitter processing needs five times more real multiplications than plain CP-OFDM without channel filtering. The FC-F-OFDM processing complexity is still significantly smaller than with direct time domain filtering implementation achieving similar level of spectral containment [40]. Furthermore, FC-F-OFDM processing provides flexibility in allocation granularity that is not easily managed with time domain filter applications. Due to the complexity and depending on the forthcoming 3GPP 5G NR inband and out-of-band emission requirements it is expected that WOLA can be used in most cases, but FC-F-OFDM should be evaluated as the 2nd generation implementation solution for 5G NR basestations and possibly in user equipment at some point [40]. Furthermore, FC-F-OFDM processing provides flexibility in allocation granularity that is not easily managed with time domain filter applications. Due to the complexity and depending on the forthcoming 3GPP 5G NR inband and out-of-band emission requirements it is expected that WOLA can be used in most cases, but FC-F-OFDM should be evaluated as the 2nd generation implementation solution for 5G NR basestations and possibly in user equipment at some point.

7. LINK PERFORMANCE EVALUATION

In this chapter, overall link level performance results for FC-F-OFDM and W-OFDM are presented and analyzed. Enhanced CP-OFDM waveforms are compared against LTE-like reference waveforms (presented in Section 5.1) in terms of BLER performance as a function of link SNR. First, the parameters and assumptions related to link level simulations are presented. Then, various transmitting scenarios are considered, including interferences and interference-free transmissions following the 3GPP calibration simulation assumptions described in [13], in order to study versatility of waveform characteristics.

7.1 Simulations cases

All results presented in this section assume an ideal channel knowledge in the receiver side and each simulated subframes contains only data symbols (no reference/pilot symbols) for simplicity. The baseline physical layer definition and numerology listed in 5.1, follows the one defined for LTE operating in a 10 MHz channel (explained in Section 5.2.1). Extending fullband allocation would not have huge effect here as interference scenarios uses 4 PRB allocation, when only the length of the fullband filter would change. Hence, the maximum allocation size of 50 PRB is used in all simulations. Single tap channel estimator and equalizer are used here per subcarrier. The used carrier frequency is 4 GHz and the Rx mobility is set to 3 km/h. Channel codec is a turbo codec following the LTE specification [48]. Single-input single-output (SISO) antenna scheme i.e. one Tx and Rx antenna is used here. Multi-antenna techniques are out of the scope of this thesis and are possible topics for future research related to results obtained here.

The link performance results are provided for DL and UL following the simulation cases defined in [13]. In uplink simulations, DFTs-OFDM is also evaluated as it is utilized in current LTE UL. These cases are targeted to satisfy New Radio requirements, which are listed in technical report TR 38.802 [13]. It also defines that bandwidth efficiency higher than the current 90% in LTE [46], should be enabled by the specification and that mixing different numerologies and services inside one channel should be enabled. Therefore, the focus here is to evaluate performance in pres-

ence of interferers in a single (asynchronous transmission) and a mixed numerology (synchronous transmission) cases. In mixed numerology cases the interfering signals have a different subcarrier spacing. If the signal with higher SCS is located on the baseline 15 kHz frequency raster, it leads to unequal interference distribution on different sides of the higher SCS allocation. Hence, the interfering signal is centered within the allocation, and thus is not anymore aligned with the baseline 15 kHz frequency raster. This provides equal interference leakage outside the allocation in both sides of the signal. All cases are evaluated over two different channel models, TDL-C-300 and TDL-C-1000, which are described in Section 5.3.

7.1.1 Case 1, interference free scenario

The first case is a simple transmission scheme without any interferers. As there is only one transmission, Case 1a and 1b are naturally single numerology cases. 1a is a downlink transmission scheme transmitting fullband signal of 50 PRBs, which is illustrated in Figure 7.1 (a). Fullband allocation of 50 PRB is selected to correspond LTE specification for 10 MHz channel bandwidth [15]. Uplink single numerology scheme is denoted here as Case 1b. It is assumed that only one UE with narrow bandwidth (4 PRB allocation) is active and that UE is located at the edge of wide frequency band as illustrated in Figure 7.1 (b).

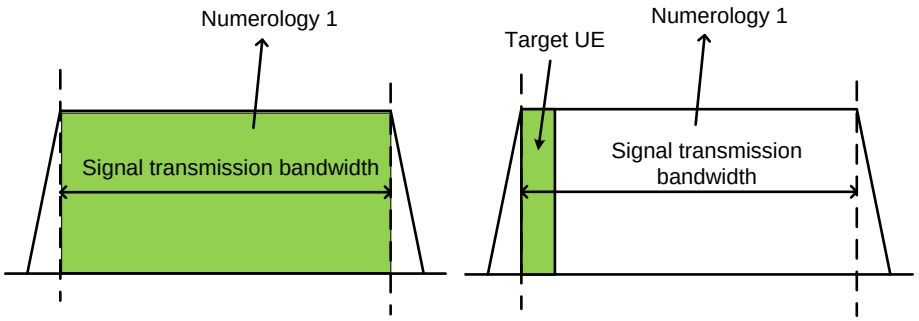

(a) Case 1a. (b) Case 1b.

Figure 7.1 *Case 1, interference free (a) DL and (b) UL transmission schemes.*

MCS for DL fullband scheme is set to 256-QAM, $R = 4/5$ as it tries to maximize throughput of the transmission. Rapp PA model is used here, as it is defined for DL simulations. Input backoff for each waveform was set to be constant $IBO = 11.6$ dB in order to provide 46 dBm total output power from the PA output (see Section 5.4.1). It was earlier examined (see Figure 6.2), that waveforms considered in this thesis, fulfils the DL OBE mask defined for LTE with 50 PRB fullband allocation.

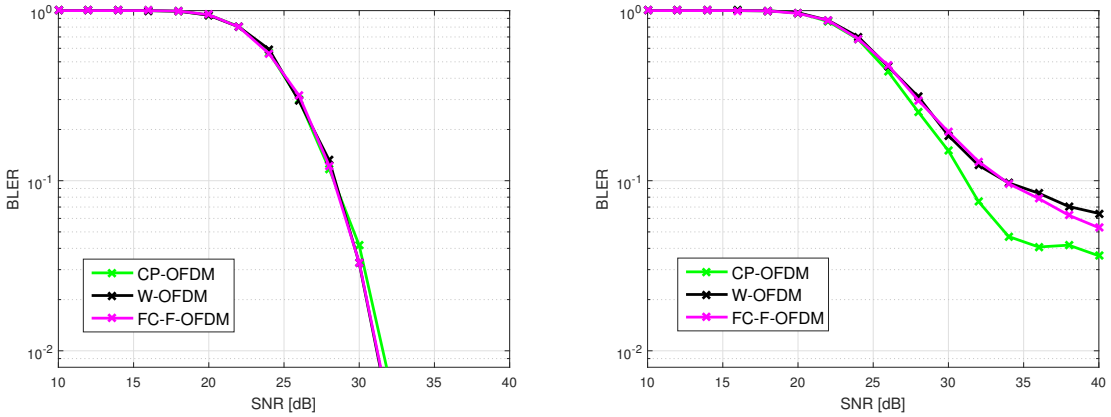

(a) Case 1a, TDL-C-300 channel.

(b) Case 1a, TDL-C-1000 channel.

Figure 7.2 *Case 1a, fullband DL link performance for (a) TDL-C-300 and (b) TDL-C-1000 channels.*

The DL performance of the FC-F-OFDM and W-OFDM are compared against CP-OFDM in TDL-C-300 and TDL-C-1000 channels shown in Figure 7.2 (a) and Figure 7.2 (b), respectively. In TDL-C-300 channel, all waveform candidates perform well in DL with MCS 256-QAM, $R = 4/5$ with 50 PRB fullband allocation, and no significant difference between waveforms is observed. The short delay spread of the channel does not produce harmful multipath components, and channel induced ISI can be compensated well with the used CP. In TDL-C-1000 channel, where delay spread is significantly longer, ISI caused by channel start to have a significant role. Hence, the differences between waveform candidates become more clear in TDL-C-1000 channel as seen in Figure 7.2. It can be seen that CP-OFDM have slightly better performance than FC-F-OFDM, which is due to the different filter lengths. Channel filtering has shorter filter than the filter used in FC-F-OFDM, which has transition bandwidth of only 3 frequency bins i.e. subcarriers. In the case of channel filtering implementation with FC-F-OFDM for 50 to 54 PRB allocations, it would be better to use 7 frequency bin transition bands to reduce the ISI effect caused by the TDL-C-1000 channel

In uplink scheme, MCS is reduced to 64-QAM, $R = 3/4$ and the PA model is switched to Polynomial PA model. Allocation size is 4 PRB, which corresponds to 720 kHz transmission bandwidth. IBO values for 4 PRB UL scenario is examined in Section 6.2.2 and are listed here in Table 7.1. Results for Case 1b are shown in Figures 7.3 (a) and 7.3 (b) for TDL-C-300 and TDL-C-1000 channels, respectively.

It can be noted that in TDL-C-300 channel, W-OFDM and FC-F-OFDM have

Table 7.1 *Waveform specific IBO values for 4 PRB UL simulations.*

Waveform	IBO [dB]
CP-OFDM	12.5
W-OFDM	12.5
FC-F-OFDM	12.8
DFTs-OFDM	11.0

similar UL link performance as CP-OFDM. Poor performance of DFTs-OFDM is due to the one tap channel estimator and equalizer structure. That is suitable for OFDM multicarrier techniques, where high interference in one frequency tap affects only to one symbol. In DFTs-OFDM, this interference is spread over all symbols, and thus, the performance is degraded significantly. More complex equalizers can be used with DFTs-OFDM, but in these simulation conditions its performance is clearly weakest.

In TDL-C-1000 channel, ISI caused by the channel is more significant and differences between waveforms are more considerable. While DFTs-OFDM having poorest performance, CP-OFDM have slightly better performance than FC-F-OFDM for same filter length related reasons than in Case 1a. Performance of W-OFDM does not differ significantly form FC-F-OFDM results and the differences between all waveforms (except DFTs-OFDM) are rather small in terms of BLER.

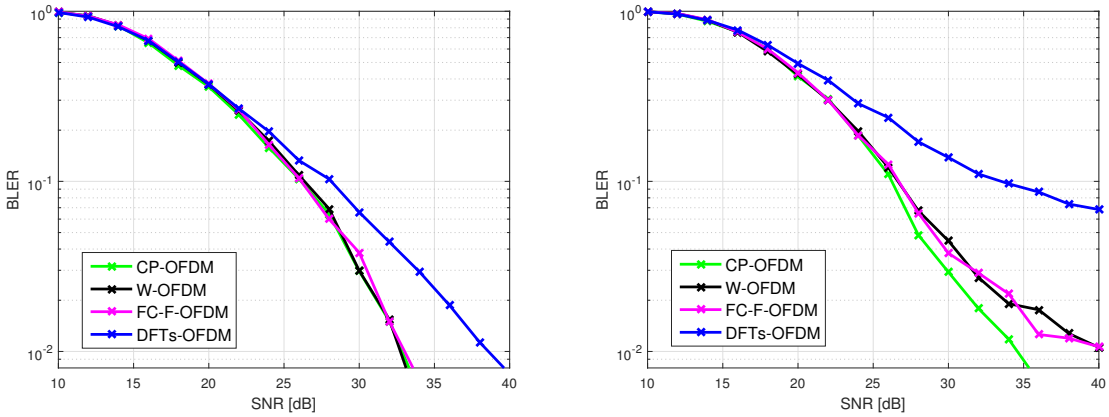

(a) Case 1b, TDL-C-300 channel.

(b) Case 1b, TDL-C-1000 channel.

Figure 7.3 *Case 1b UL link performance for (a) TDL-C-300 and (b) TDL-C-1000 channels.*

It is desirable that new proposed waveforms have similar performance in interference free scenarios than the current LTE waveform based on channel filtering. It

should be noted that W-OFDM and FC-F-OFDM are designed for narrow bandwidths as well, which emerges better in presence of interferences.

7.1.2 Case 2, downlink mixed numerology

Case 2 is a mixed numerology case in downlink transmission scheme with 4 PRB allocation. In DL, more linear PA model allows to use higher MCS and 256-QAM, $R = 3/4$ is used here. The target user is located at the edge of the target subband (see Figure 7.4), which is interfered by the neighboring subband. Timing synchronization between desired and interfering subband is retained, but used numerologies are different causing additional interference. Interfering signal has SCS of 30 kHz in order to model interference from a different numerology signal transmitted to another UE using different service than the target UE. The used MCS is 256-QAM, $R = 3/4$ and IBO value is 11.6 dB for DL interfering signal.

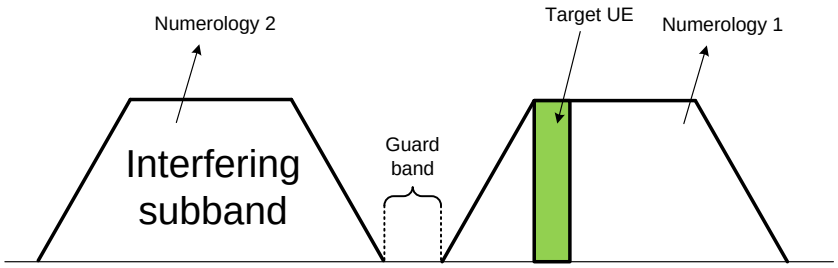

Figure 7.4 *Case 2, mixed numerology transmission scheme with guard band.*

In addition to link level BLER performance, effect of guard band between desired and interfering subband are shown. GBs of 0 kHz, 90 kHz and 180 kHz are plotted in solid line with marker, dashed line and dashed line with marker, respectively. Typically the required GB is smaller than in the corresponding UL scenario, due to the more linear PA model. Result for Case 2 are shown for TDL-C-300 in Figure 7.5 (a) and for TDL-C-1000 in Figure 7.5 (b).

In presence of interference from a different numerology, MCS of 256-QAM, $R = 4/5$ does not work without guard band as it is more sensitive to distortions than 64-QAM, 3/4. The side lobes of the interfering subband are not suppressed enough and the link performance in both channels are very poor, resulting BLER values close to 1. When guard band is added, the link performance is improved significantly, especially in TDL-C-300 channel. FC-F-OFDM has clearly the best performance, due to the good filtering characteristics and 90 kHz guard band is already enough to achieve best BLER performance among waveform candidates. Adding more GB does

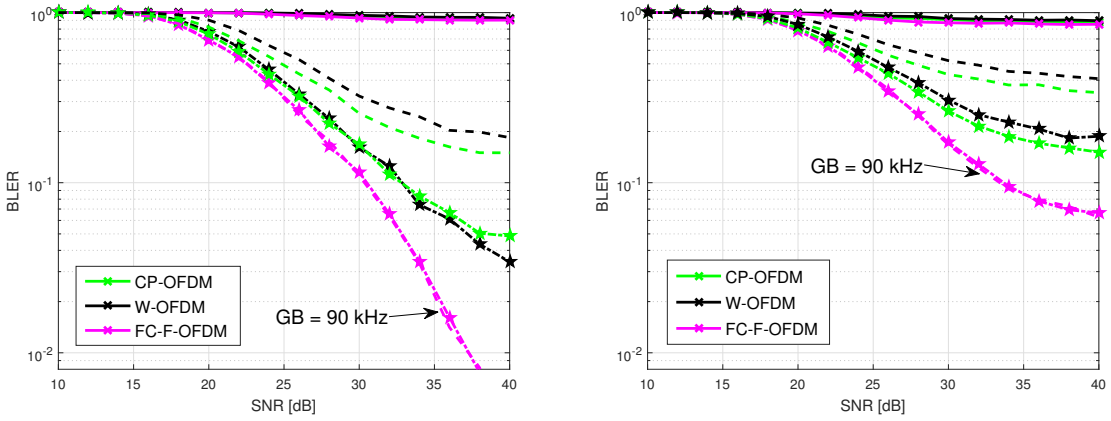

(a) Case 2, TDL-C-300 channel.

(b) Case 2, TDL-C-1000 channel.

Figure 7.5 *Case 2 DL link performance with GBs of 0, 90 and 180 kHz for (a) TDL-C-300 and (b) TDL-C-1000 channels.*

not improve the BLER performance of FC-F-OFDM due to the effective filtering, which can be seen as a overlapping lines in Figure 7.5 (a) (90 kHz GB dashed line is highlighted with text arrow). As the W-OFDM does not suppress side lobes as effectively as FC-F-OFDM, the guard band of 90 kHz is not enough to achieve 10% BLER performance even with high SNR values. With guard band of 180 kHz, W-OFDM performs slightly better than CP-OFDM, but differences between W-OFDM and CP-OFDM are minimal. These results are in line with the inband ACLR results, although obtained for UL, shown in Table 6.10 where it was observed that the leakage power from CP-OFDM and W-OFDM are rather similar with guard band 180 kHz. In TDL-C-1000 channel, similar trends are observed in the results, but BLER performance is poorer due to the ISI caused by the channel. FC-F-OFDM has a similar performance with 90 kHz and 180 kHz GBs. It can be said that the FC-F-OFDM is only waveform which can used in TDL-C-1000 channel with 256-QAM as the other candidates can not achieve 10% BLER performance even with 180 kHz guard band. It is also noted that W-OFDM performance is here worse than CP-OFDM.

7.1.3 Case 3, asynchronous uplink

Uplink single numerology scheme is evaluated in Case 3. Target UE has interferers in both sides as illustrated in Figure 7.6. These interferers have same numerology than target UE (SCS of 15 kHz), which models the transmission scheme of three neighboring signals originated from different user equipments using same SCS. Only

the target UE is evaluated while the other two UEs are considered as interferers. Interfering signal is time shifted with 128 samples to model asynchronous interference scheme.

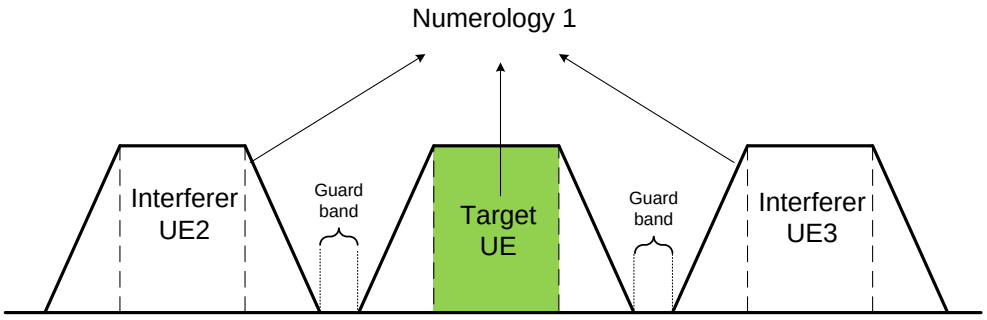

Figure 7.6 *Case 3, single numerology transmission scheme with guard bands.*

MCS 64-QAM, $R = 1/2$ is used for desired signal and IBO values for each waveforms are listed in Table 7.1 (evaluated in Section 6.2.2). The interfering signals use MCS 256-QAM, $R = 3/4$ with IBO of 5.5 dB. The link performance results in Case 3 asynchronous UL scenario are shown in Figures 7.7 (a) and 7.7 (b) for TDL-C-300 and TDL-C-1000 channels, respectively. GBs of 0 Hz and 90 kHz between the desired signal and the interfering signals in both sides are used. Solid lines with x-marker and dashed lines represents the link performance with 0 Hz and 90 kHz guard bands, respectively.

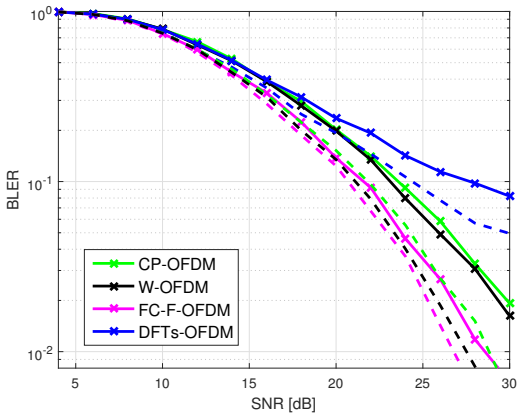

(a) Case 3, TDL-C-300 channel.

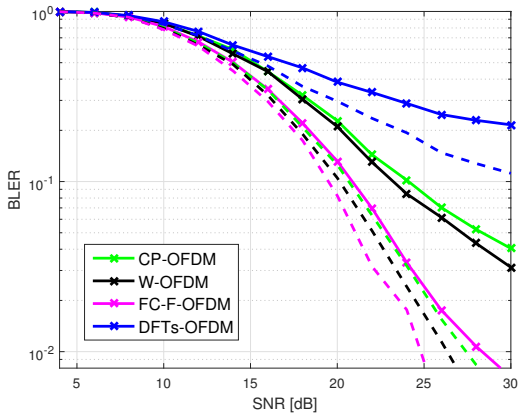

(b) Case 3, TDL-C-1000 channel.

Figure 7.7 *Case 3, asynchronous UL scheme with GBs of 0 and 90 kHz for (a) TDL-C-300 and (b) TDL-C-1000 channels.*

In presence of asynchronous interferers in the both side of the desired signal, narrowband spectrum side lobe suppression characteristics have a significant role.

While DFTs-OFDM suffering from the simple channel estimation/equalization structure here again, FC-F-OFDM has the best performance with and without a GB, as it filters effectively both sides of the 4 PRB signal spectrum (see Figure 6.6). It can be seen that without a GB, FC-F-OFDM is the only candidate to achieve 1% BLER value within the used SNR range, and thus, can be used in such conditions. GB has bigger effect on W-OFDM, that is, due to the slower suppression of the spectrum side lobes. It should be noted that W-OFDM has here better BLER performance than CP-OFDM in all scenarios although the difference is minor. However, with 90 kHz GB the differences are minor and all multicarrier waveforms (CP-OFDM, W-OFDM and FC-F-OFDM) work out well in both channels. Link performance results in TDL-C-1000 channel are similar especially in presence of guard band. Without GB, W-OFDM and CP-OFDM suffers some decrease in BLER results, whereas FC-F-OFDM can retain the similar performance also in TDL-C-1000 channel with and without GB.

7.1.4 Case 4, mixed numerology uplink

Case 4 models uplink mixed numerology case where target UE has interferers located in the both side of the desired signal, similar to Case 3. The difference is that numerology of the interfering UEs differs from target UE numerology, which models the transmission scheme of three neighboring signals originating from different services and user equipments called as mixed numerology scheme. The synchronization between subbands is now retained and there is no timing offsets between signals, which means that Case 4 is a synchronous interference scheme. This scenario is illustrated in Figure 7.8.

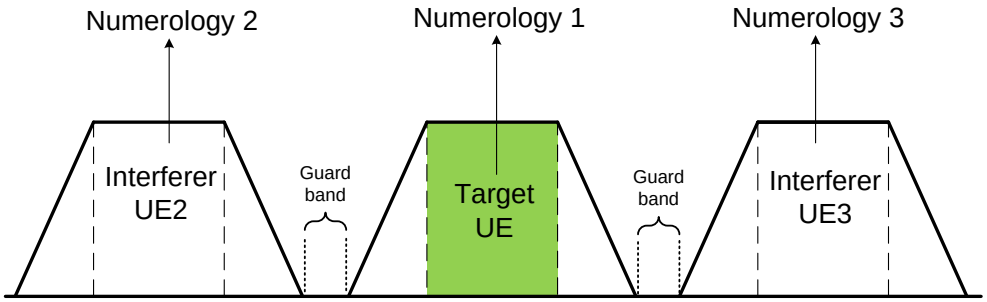

Figure 7.8 *Case 4, mixed numerology transmission scheme with guard bands.*

Equivalent to the Case 3, waveforms specific IBO values for desired signals are used corresponding to Table 7.1, and MCS 64-QAM, $R = 3/4$ is used. Both interfering signals are assumed to use SCS of 30 kHz to model interference from different

service and used MCS is 64-QAM, $R = 3/4$ with IBO of 5.5 dB. Link performance results are shown in Figure 7.9, where solid line with marker and dashed lines represents GB of 0 kHz and 90 kHz, respectively. The link performance in TDL-C-300 channel is shown in Figure 7.9 (a) and for TDL-C-1000 in Figure 7.9 (b).

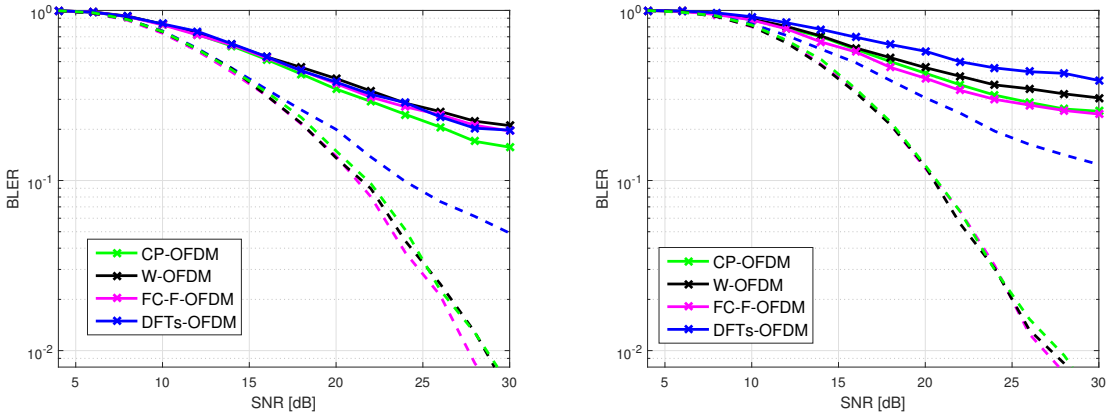

(a) Case 4, TDL-C-300 channel.

(b) Case 4, TDL-C-1000 channel.

Figure 7.9 *Case 4, synchronous mixed numerology UL scheme with GBs of 0 and 90 kHz for (a) TDL-C-300 and (b) TDL-C-1000 channels.*

In mixed numerology scenario, different SCS of the interfering signals causes significant interference to desired signal, which can be seen especially results without GB. None of the waveforms have a proper link performance with GB of 0 kHz, and BLER values are clearly over 10% for each waveform in both channels. This is due to the dominating interference originated from interfering signals having different SCS and the channel induced ISI has a minor effect to the results here. When guard band is added, link level performance is similar than in single numerology interference scheme (Case 3, Figures 7.7 (a) and 7.7 (b)). DFTs-OFDM has the worst performance similar to earlier cases. Significant differences between W-OFDM and FC-F-OFDM are not observed against CP-OFDM in Case 4. Guard band provides enough space between desired signal and interfering 30 kHz SCS, which causes minor interference to the target UE. Sidelobe suppression methods can overcome synchronous mixed interference scheme only with the guard band.

8. CONCLUSIONS

Two potential 5G NR waveforms have been studied in terms of transmitter performance including 3GPP PA models for UL and DL, as well as overall link performance with practical wireless communication conditions in all calibration scenarios defined by 3GPP. The objective was to a find new waveform processing techniques implemented on top of the CP-OFDM, which is the baseline assumption for 5G NR below 40 GHz communications, achieving good BLER performance in all link performance scenarios. Transmitter side performance has been studied to observe how the transmitter processing, especially PA processing, affects the out-of-band emissions of the evaluated waveforms. In addition, the power leakage in narrowband transmission schemes inside a wideband LTE channel was evaluated. In the following, results from Chapters 6 and 7 are summarized and conclusion is formed.

8.1 Observations based on simulations results

From the results, it can be observed that FC-F-OFDM and W-OFDM have similar fullband performance compared to channel filtered CP-OFDM, whose channel filter is designed specifically for allocation size corresponding to channel bandwidth (fullband allocation). In long delay spread channel it was observed that both W-OFDM and FC-F-OFDM have marginally worse BLER performance than CP-OFDM. With FC-F-OFDM using larger transition bandwidth is possible in the used example parametrization with maximum allocation of 50 PRBs and 54 PRBs and would improve the BLER performance. With W-OFDM reducing the time domain window length is not possible because in 50 PRB case we would violate the out-of-band emission requirements and in 54 PRBs case we are not achieving the out-of-band emission requirements even with the selected window size. Thus, additional channel filtering is needed with W-OFDM to achieve proper spectral containment in extended maximum allocation schemes.

Link level performance results also show the performance comparison between channel filtered CP-OFDM, W-OFDM and FC-F-OFDM in practical channel conditions with interference. Link performance gain is achieved in the presence of interferences, showing the better flexibility of proposed waveforms. FC-F-OFDM

has the best performance in most cases making it to desirable choice for 5G NR waveform. Also the performance can be improved with W-OFDM, which has additionally lower computational complexity. In downlink mixed numerology scheme (Case 2), FC-F-OFDM has clearly the best link performance with 90 kHz guard band and it is the only waveform to achieve 10% BLER limit. In asynchronous uplink transmission (Case 3), the FC-F-OFDM has the best BLER results without GB. When adding 90 kHz GB, the difference between waveforms are smaller, but FC-F-OFDM still having the best BLER performance. None of the waveforms are working in mixed numerology case (Case 4) without GB. Performance of all waveforms are pretty similar with 90 GB and BLER values are clearly under 10% limit. Here, UL cases (Case 3 and Case 4) uses 64-QAM as it is more sensitive to interferences. In the future 256-QAM may be used also in UL, which would bring more advantage to FC-F-OFDM link performances. It is also notable that channel filtered OFDM has rather good performance in all cases (except Case 2 in TDL-C-1000 channel) when some guard band is added. This implies that serving new services does not necessarily require new waveform, if we are prepared to use GB of 1-2 PRBs (180 kHz - 360 kHz).

In narrowband allocation, which is more 5G NR related scenario, performance increase is observed with proposed waveforms. FC-F-OFDM and W-OFDM techniques are proper also for narrowband signals as the inband power leakage is reduced in both sides. In terms of spectral power leakage the FC-F-OFDM has a better performance than W-OFDM with fullband and narrowband allocations. This implies that FC-F-OFDM requires less guard bands to support mixed service and numerology operation within eMBB channel. Assuming GB of 1 PRB (180 kHz), FC-F-OFDM have 8.8 dB higher inband ACLR value than W-OFDM. In addition, FC-F-OFDM is the only waveform to achieve 30 dB UL ACLR requirement with GB of 1 PRB. Therefore, demands for future traffic trends are better fulfilled with FC-F-OFDM as the IoT and M2M -type of communications are envisioned to increase in the future.

Although the FC-F-OFDM appears to be better option in terms of power leakage, the computational complexity - which is evaluated in terms of number of real multiplications - is higher in transmitter processing. FC-F-OFDM processing requires over 5 times higher computational capacity per symbol than conventional CP-OFDM processing without channel filtering. In practise, the difference is smaller because CP-OFDM always requires channel filtering. W-OFDM has a significantly lower processing complexity adding only 1.7% real multiplications per symbol compared

to conventional CP-OFDM without channel filtering. This increases the interest for W-OFDM as it has also proper narrowband power leakage characteristics. When making the final decision, the trade-off between waveforms spectral containment and complexity should be done to obtain the best performing solution while fulfilling the requirements of the system in question.

8.2 Future studies

In this thesis, single-input single-output scheme is assumed. As the OFDM technique is well suited for multi-antenna transmission schemes, multiple-input multiple-output scheme is a crucial part of the 5G research. Adding more antennas to the transmission scheme enables to use additional signal combining techniques in order to decrease interferences, and thus, to achieve higher reliability or multiple spatial streams can be supported to improve transmission rates. The next step to continue this study could be simulations using various MIMO schemes and to compare candidate waveforms performance with MIMO techniques against the SISO results provided here.

High PAPR values being the main drawback of the OFDM based multicarrier waveforms, additional PAPR reduction techniques are typically added to the waveform processing. With lower PAPR, multicarrier techniques could be used more widely in uplink, which would be a desirable scheme to simplify the network functionality. When using e.g. peak clipping to reduce PAPR value of the multicarrier waveform, the PA non-linearities are reduced and higher transmission powers can be used. Adding PAPR reduction techniques to the transmitter processing could bring new aspects to the waveform analysis as they typically increase EVM and out-of-band power leakage.

BIBLIOGRAPHY

[1] T. Wild, F. Schaich, and Y. Chen. "5G air interface design based on Universal Filtered (UF-)OFDM". In *2014 19th International Conference on Digital Signal Processing*, pages 699–704, Aug 2014.

[2] Mikko Maenpaa. "Blind Detection of Interfering Cell Data Channel Power Level in 3GPP LTE/LTE-A Downlink". Master's thesis, Tampere University of Technology, 2015.

[3] Nokia. "5G Radio Access - System Design Aspects", 2015. Online: `http://resources.alcatel-lucent.com/asset/200009`, last accessed 7th April 2017.

[4] G. Wunder, P. Jung, M. Kasparick, T. Wild, F. Schaich, Y. Chen, S. T. Brink, I. Gaspar, N. Michailow, A. Festag, L. Mendes, N. Cassiau, D. Ktenas, M. Dryjanski, S. Pietrzyk, B. Eged, P. Vago, and F. Wiedmann. 5GNOW: non-orthogonal, asynchronous waveforms for future mobile applications. *IEEE Communications Magazine*, 52(2):97–105, February 2014.

[5] J. Vihriälä, A. A. Zaidi, V. Venkatasubramanian, N. He, E. Tiirola, J. Medbo, E. Lähetkangas, K. Werner, K. Pajukoski, A. Cedergren, and R. Baldemair. "Numerology and frame structure for 5G radio access". In *2016 IEEE 27th Annual International Symposium on Personal, Indoor, and Mobile Radio Communications (PIMRC)*, pages 1–5, Sept 2016.

[6] K. Ganesan, T. Soni, S. Nunna, and A. R. Ali. "Poster: A TDM approach for latency reduction of ultra-reliable low-latency data in 5G". In *2016 IEEE Vehicular Networking Conference (VNC)*, pages 1–2, Dec 2016.

[7] Rath Vannithamby and Shilpa Talwar. *"Towards 5G: Applications, Requirements and Candidate Technologies"*. John Wiley & Sons, Jan 2017.

[8] M. Abdelaziz, L. Anttila, M. Renfors, and M. Valkama. "PAPR reduction and digital predistortion for non-contiguous waveforms with well-localized spectrum". In *2016 International Symposium on Wireless Communication Systems (ISWCS)*, pages 581–585, Sept 2016.

[9] G. Berardinelli, K. Pajukoski, E. Lahetkangas, R. Wichman, O. Tirkkonen, and P. Mogensen. "On the Potential of OFDM Enhancements as 5G Waveforms". In *2014 IEEE 79th Vehicular Technology Conference (VTC Spring)*, pages 1–5, May 2014.

[10] Qualcomm. "5G Waveform & Multiple Access Techniques", 2015. Online: https://www.qualcomm.com/media/documents/files/5g-research-on-waveform-and-multiple-access-techniques.pdf, last accessed 7th April 2017.

[11] J. Luo, W. Keusgen, and A. Kortke. "Optimization of Time Domain Windowing and Guardband Size for Cellular OFDM Systems". In *Vehicular Technology Conference, 2008. VTC 2008-Fall. IEEE 68th*, pages 1–5, Sept 2008.

[12] A. Sahin and H. Arslan. "Edge Windowing for OFDM Based Systems". *IEEE Communications Letters*, 15(11):1208–1211, November 2011.

[13] 3rd Generation Partnership Project; Technical Specification Group Radio Access Network; Study on New Radio (NR) Access Technology Physical Layer Aspects (Release 14), document 3GPP TR 38.802 V14.0.0 (2017-03).

[14] Richard van Nee and Ramjee Prasad. *"OFDM for Wireless Multimedia Communications"*. Artech House, Inc., Norwood, MA, USA, 1st edition, 2000.

[15] Erik Dahlman, Stefan Parkvall, and Johan Skold. *"4G: LTE/LTE-Advanced for Mobile Broadband"*. Academic Press, 1st edition, 2011.

[16] G. Liu and J. Zhang. "Comparative Investigation on MU-MIMO Schemes for TDD MIMO OFDMA Uplink". In *2006 International Conference on Wireless Communications, Networking and Mobile Computing*, pages 1–4, Sept 2006.

[17] X. Hong, J. Wang, C. X. Wang, and J. Shi. "Cognitive radio in 5G: a perspective on energy-spectral efficiency trade-off". *IEEE Communications Magazine*, 52(7):46–53, July 2014.

[18] B. Farhang-Boroujeny. "OFDM Versus Filter Bank Multicarrier". *IEEE Signal Processing Magazine*, 28(3):92–112, May 2011.

[19] A. E. Loulou, S. Afrasiabi Gorgani, and M. Renfors. "Enhanced OFDM techniques for fragmented spectrum use". In *Future Network and Mobile Summit (FutureNetworkSummit), 2013*, pages 1–10, July 2013.

[20] Fa-Long Luo. *"Digital Front-End in Wireless Communications and Broadcasting: Circuits and Signal Processing"*. Cambridge University Press, Aug 2011.

[21] F. M. Ghannouchi and O. Hammi. "Behavioral modeling and predistortion". *IEEE Microwave Magazine*, 10(7):52–64, Dec 2009.

[22] Multicarrier and Multiantenna Techniques. "*RF imperfections*", 2016. Tampere University of Technology. Limited availability.

[23] R. Prasad. *"OFDM for Wireless Communications Systems"*. Artech House universal personal communications series. Artech House, 2004.

[24] F. Lu, M. Xu, L. Cheng, J. Wang, S. Shen, J. Zhang, and G. K. Chang. "Sub-Band Pre-Distortion for PAPR Reduction in Spectral Efficient 5G Mobile Fronthaul". *IEEE Photonics Technology Letters*, 29(1):122–125, Jan 2017.

[25] A. Wakeel and W. Henkel. "Multi-edge-type LDPC code concatenated with Trellis Shaping for PAR reduction". In *2016 9th International Symposium on Turbo Codes and Iterative Information Processing (ISTC)*, pages 246–250, Sept 2016.

[26] S. H. Aswini, B. N. A. Lekshmi, S. Sekhar, and S. S. Pillai. "MIMO-OFDM frequency offset estimation for Rayleigh fading channels". In *Computational Systems and Communications (ICCSC), 2014 First International Conference on*, pages 191–196, Dec 2014.

[27] Songping Wu and Y. Bar-Ness. "OFDM systems in the presence of phase noise: consequences and solutions". *IEEE Transactions on Communications*, 52(11):1988–1996, Nov 2004.

[28] Alaaeddin Loulou. "Enchanched OFDM for Fragmented Spectrum Use". Master's thesis, Tampere University of Technology, 2013.

[29] T. Weiss, J. Hillenbrand, A. Krohn, and F. K. Jondral. "Mutual interference in OFDM-based spectrum pooling systems". In *Vehicular Technology Conference, 2004. VTC 2004-Spring. 2004 IEEE 59th*, volume 4, pages 1873–1877 Vol.4, May 2004.

[30] 3rd Generation Partnership Project; Technical Specification Group Radio Access Network; Feasibility Study for Orthogonal Frequency Division Multiplexing (OFDM) for UTRAN enhancement (Release 6), document 3GPP TR 25.892 V6.0.0 (2004-06).

[31] AlaaEddin Loulou and Markku Renfors. "Enhanced OFDM for Fragmented Spectrum Use in 5G Systems". *Trans. Emerg. Telecommun. Technol.*, 26(1):31–45, January 2015.

[32] J. Abdoli, M. Jia, and J. Ma. "Filtered OFDM: A new waveform for future wireless systems". In *2015 IEEE 16th International Workshop on Signal Processing Advances in Wireless Communications (SPAWC)*, pages 66–70, June 2015.

[33] J. Li, K. Kearney, E. Bala, and R. Yang. "A resource block based filtered OFDM scheme and performance comparison". In *Telecommunications (ICT), 2013 20th International Conference on*, pages 1–5, May 2013.

[34] X. Zhang, M. Jia, L. Chen, J. Ma, and J. Qiu. "Filtered-OFDM - Enabler for Flexible Waveform in the 5th Generation Cellular Networks". In *2015 IEEE Global Communications Conference (GLOBECOM)*, pages 1–6, Dec 2015.

[35] Waveform Candidates, 3GPP TSG RAN WG1 meeting #84b, R 1-162199, Busan, Korea, Apr, 11-15, 2016.

[36] F. Schaich, T. Wild, and Y. Chen. "Waveform Contenders for 5G - Suitability for Short Packet and Low Latency Transmissions". In *2014 IEEE 79th Vehicular Technology Conference (VTC Spring)*, pages 1–5, May 2014.

[37] T. Wild, F. Schaich, and Y. Chen. "5G air interface design based on Universal Filtered (UF-)OFDM". In *2014 19th International Conference on Digital Signal Processing*, pages 699–704, Aug 2014.

[38] M. Renfors, J. Yli-Kaakinen, T. Levanen, M. Valkama, T. Ihalainen, and J. Vihriala. "Efficient Fast-Convolution Implementation of Filtered CP-OFDM Waveform Processing for 5G". In *2015 IEEE Globecom Workshops (GC Wkshps)*, pages 1–7, Dec 2015.

[39] Juha Yli-Kaakinen and Markku Renfors. "Optimization of flexible filter banks based on fast convolution". *Journal of Signal Processing Systems*, 85(1):101–111, August 2016.

[40] J. Yli-Kaakinen, T. Levanen, S. Valkonen, K. Pajukoski, J. Pirskanen, M. Renfors, and M. Valkama. "Efficient Fast-Convolution Based Waveform Processing for 5G Physical Layer". *IEEE Journal on Selected Areas in Communications*, PP(99):1–1, 2017.

[41] A. Daher, E. H. Baghious, G. Burel, and E. Radoi. "Overlap-Save and Overlap-Add Filters: Optimal Design and Comparison". *IEEE Transactions on Signal Processing*, 58(6):3066–3075, June 2010.

[42] Lawrence R. Rabiner and Bernard Gold. *"Theory and Application of Digital Signal Processing"*. Englewood Cliffs, NJ: Prentice-Hall, 1975.

[43] M. Renfors, J. Yli-Kaakinen, and F. Harris. "Analysis and design of efficient and flexible fast-convolution based multirate filter banks". *IEEE Trans. Signal Processing*, 62(15):3768–3783, August 2014.

[44] M. Renfors, J. Yli-Kaakinen, and M. Valkama. "Power Amplifier Effects on Frequency Localized 5G Candidate Waveforms". In *European Wireless 2016; 22th European Wireless Conference*, pages 1–5, May 2016.

[45] Dr Harri Holma and Dr Antti Toskala. *"LTE for UMTS - OFDMA and SC-FDMA Based Radio Access"*. Wiley Publishing, 2009.

[46] 3rd Generation Partnership Project; Technical Specification Group Radio Access Network; Evolved Universal Terrestrial Radio Access (E-UTRA) and Evolved Universal Terrestrial Radio Access Network (E-UTRAN); Overall Description; Stage 2 (Release 13), document 3GPP TS 36.300 V13.4.0 (2016-07).

[47] 3rd Generation Partnership Project; Technical Specification Group Radio Access Network; Study on New Radio Access Technology: RF and co-existence aspects (Release 14), document 3GPP TR 38.803 V14.0.0 (2017-03).

[48] 3rd Generation Partnership Project; Technical Specification Group Radio Access Network; Evolved Universal Terrestrial Radio Access (E-UTRA); Base Station (BS) Radio Transmission and Reception (Release 13), document 3GPP TS 36.104 V14.1.0 (2016-10).

[49] 3rd Generation Partnership Project; Technical Specification Group Radio Access Network; Evolved Universal Terrestrial Radio Access (E-UTRA); User Equipment (UE) Radio Transmission and Reception (Release 13), document 3GPP TS 36.101 V13.3.0 (2016-03).

[50] R1-167963, Way forward on waveform, 2016. 3GPP TSG-RAN WG1 Meeting #86, Online: `www.3gpp.org/ftp/tsg_ran/WG1_RL1/TSGR1_86/Docs/`, last accessed 7th April 2017.

[51] 3rd Generation Partnership Project; Technical Specification Group Radio Access Network; Study on channel model for frequency spectrum above 6 GHz, document 3GPP TR 38.900 V14.0.0 (2016-06).

[52] Alcatel-Lucent Shanghai Bell Nokia. "R1-167297, [85-18] PA assumptions for NR; Email discussion summary", 2016. 3GPP TSG-RAN WG1#86, Online: `http://www.3gpp.org/ftp/tsg_ran/WG1_RL1/TSGR1_86/Docs/`, last accessed 7th April 2017.

[53] T. Saynajakangas. "R1-166004, Response LS on realistic power amplifier model for NR waveform evaluation", 2016. 3GPP TSG-RAN WG1 Meeting #86, Online: `http://www.3gpp.org/ftp/tsg_ran/WG1_RL1/TSGR1_85/Docs/`, last accessed 7th April 2017.

[54] ITU-R recommendation SM.329: "Unwanted emissions in the spurious domain".

[55] H. Sorensen, M. Heideman, and C. Burrus. "On computing the split-radix FFT". *IEEE Transactions on Acoustics, Speech, and Signal Processing*, 34(1):152–156, Feb 1986.